Published in final edited form as:
J Mol Biol. 2011 July 8; 410(2): 241–267. doi:10.1016/j.jmb.2011.04.001.

Nonspecific DNA Binding and Bending by $HU_{\alpha\beta}$: Interfaces of the Three Binding Modes Characterized by Salt Dependent Thermodynamics

Junseock Koh[1,*], **Irina Shkel**[2], **Ruth M. Saecker**[2], and **M. Thomas Record Jr.**[1,2,3,*]

[1]Program in Biophysics, University of Wisconsin, Madison WI 53706

[2]Department of Chemistry, University of Wisconsin, Madison WI 53706

[3]Department of Biochemistry, University of Wisconsin, Madison WI 53706

Abstract

Previous ITC and FRET studies demonstrated that *Escherichia coli* $HU_{\alpha\beta}$ binds nonspecifically to duplex DNA in three different binding modes: a tighter-binding 34 bp mode which interacts with DNA in large (>34 bp) gaps between bound proteins, reversibly bending it 140° and thereby increasing its flexibility, and two weaker, modestly cooperative small-site-size modes (10 bp, 6 bp) useful for filling gaps between bound proteins shorter than 34 bp. Here we use ITC to determine the thermodynamics of these binding modes as a function of salt concentration, and deduce that DNA in the 34 bp mode is bent around but not wrapped on the body of HU, in contrast to specific binding of IHF. Analyses of binding isotherms (8, 15, 34 bp DNA) and initial binding heats (34, 38, 160 bp DNA) reveal that all three modes have similar log-log salt concentration derivatives of the binding constants (Sk_i) even though their binding site sizes differ greatly; most probable values of Sk_i on 34 bp or larger DNA are -7.5 ± 0.5. From the similarity of Sk_i values, we conclude that binding interfaces of all three modes involve the same region of the arms and saddle of HU. All modes are entropy-driven, as expected for nonspecific binding driven by the polyelectrolyte effect. The bent-DNA 34 bp mode is most endothermic, presumably because of the cost of HU-induced DNA bending, while the 6 bp mode is modestly exothermic at all salt concentrations examined. Structural models consistent with the observed Sk_i values are proposed.

Introduction

Escherichia coli $HU_{\alpha\beta}$ and its structural homolog IHF are major nucleoid associated-proteins (NAPs) in all phases of cell growth. Both HU and IHF function in various DNA transactions, including DNA compaction, recombination, and transcription, by modifying DNA conformation (e.g., bending, looping) [1; 2; 3; 4; 5]. Comparisons of thermodynamic and structural properties of HU and IHF in binding to duplex DNA are needed for a molecular understanding of similarities and differences in the physiological roles of these structurally homologous proteins: why does the cell retain both proteins in spite of their very similar architecture, and co-regulate the amounts of two proteins as a function of growth

[*]corresponding authors: 433 Babcock Drive, Madison, WI 53706, Phone: 608-262-5332, FAX: 608-262-3453, mtrecord@wisc.edu; 1230 York Avenue, New York, NY 10065, Phone: 212-327-8181, FAX: 212-327-7880, jkoh@rockefeller.edu.

phase [6; 7; 8]? In addition, HU and/or IHF may serve as experimentally-tractable model systems to investigate structural and thermodynamic aspects of assembly and function of larger nucleoprotein complexes which involve significant bending or wrapping of DNA around protein surface, including the nucleosome [9].

Our previous ITC and FRET studies [10] of the nonspecific interactions between HU and duplex DNA oligomers in the length range 8 bp – 160 bp provide a comprehensive, quantitative framework for understanding and unifying previously-reported, sometimes contrasting effects of HU on DNA conformation (e.g. compaction, extension) and the DNA binding properties of HU (including site size, binding constant, cooperativity) observed in single molecule [11; 12; 13] and bulk solution studies [14; 15; 16; 17; 18; 19; 20]. At 0.15 M Na^+ and 15 °C, we deduced that HU binds duplex DNA in three different modes depending on the ratio of total concentrations of HU to DNA ($[HU]_{total}/[DNA]_{total}$, abbreviated hereafter as [HU]/[DNA]) and DNA length. These modes differ in binding site size, binding constant, and binding enthalpy. Decreasing [HU]/[DNA] at constant DNA length or increasing DNA length at low [HU]/[DNA] drives binding mode transitions from smaller site size modes (e.g., smaller number of DNA base pairs occluded by HU) to larger site size modes. Our ITC characterization (at 15 °C and 0.15 M Na^+) of the binding mode with the largest site size revealed that it occludes 34 bp and is the most endothermic (+ 7.7 kcal/mol). FRET studies using fluorescent probes at the ends of a 34 bp duplex DNA showed that the 34 bp mode bends the DNA by ~ 140°. The other two modes with smaller binding site sizes occlude 10 bp and 6 bp with binding enthalpies of + 4.2 kcal/mol and − 1.6 kcal/mol, respectively, exhibit moderate intra- and intermode cooperativities, and do not induce detectable bending of a 34 bp duplex DNA in a FRET assay. Based on the binding mode transitions we observed as a function of [HU]/[DNA] ratio and DNA length, we proposed that the tighter-binding 34 bp mode interacts with vacant regions of nucleoid DNA in large (< 34 bp) gaps between bound proteins, reversibly bending it 140° and thereby increasing its flexibility, and that the two weaker, modestly cooperative small-site-size modes (10 bp, 6 bp) are used to fill gaps shorter than 34 bp between bound proteins.

No crystal or solution structure has yet been determined for any of these three nonspecific binding modes of HU, probably because binding constants are modest and competition between the modes leads to a mixed population of complexes under most conditions. The crystal structure of a tighter-binding complex of *Anabaena* HU with a duplex DNA 17-mer with 3 mismatched T:T appositions and 4 unpaired T [21] (see Fig. 8a) appears useful as a model for the 34 bp mode detected in our previous ITC and FRET studies, based on their similar binding site sizes and DNA bend angles [10]. In the crystal structure, the β – saddle/arm region from each monomer binds the minor groove at the central region of the DNA spanning ~ 10 bp. The conserved proline residues at the tips of the arms insert between DNA base pairs at the ends of the central 10 bp region, inducing sharp bending of the 5′- and 3′-terminal regions flanking the proline insertion points toward the α-helical body region of HU. Steric considerations based on the highly bent DNA trajectory suggested that binding of one HU could occlude up to 35 bp of a longer DNA even if the flanking DNA was not wrapped on the body of HU [1; 6; 21]. The 10 bp mode has been proposed to utilize the central portion of the binding interface observed in the crystal structure: the β – saddle/arms of HU interact with one helical turn (~ 10 bp) of the DNA minor groove without proline insertion/DNA bending [6; 14; 16; 22]. No structural prediction has been made for the 6 bp mode.

Comprehensive thermodynamic studies for dependences of DNA binding mode transitions on solution variables have been reported for single strand DNA binding proteins from *E.coli* (SSB) [23; 24; 25; 26] and from *Saccahromyces cerevisiae* (scRPA) [27] and for human or rat DNA polymerase β [28; 29]. Until recently [10], no corresponding information has been available for nonspecific binding of any NAP to double stranded DNA. For SSB and scRPA, changes

in solution variables such as salt concentration and type, pH, and temperature are major driving forces for the binding mode transitions in addition to the [protein]/[DNA] mole ratio and DNA length [23; 25; 27]. In particular, both proteins exhibit remarkable changes in binding modes with varying salt concentration; small site size modes are replaced by large site size modes with increasing salt concentration. At very low or very high salt concentration, both SSB and scRPA utilize only one mode in binding to DNA. Do similar salt concentration driven binding mode transitions occur for interactions of HU with double stranded DNA?

As a first step to address the physiological and structural questions raised above, here we report the effects of salt concentration on the thermodynamic properties of the three different binding modes of HU observed in ITC data for forward titrations of 8, 15, and 34 bp DNA with HU and for initial heats of HU binding to 34, 38, and 160 bp DNA at different salt concentrations (0.06 – 0.15 M Na^+ at 15 °C). Analyses of these titrations and initial binding heats provide binding constants, binding enthalpies, and cooperativities of all three binding modes [10]. We find that the log – log salt concentration derivatives of binding constants k_i (i.e., Sk_i) for all three modes are similar within uncertainty, which indicates that the amount of salt ion release and therefore the number of DNA phosphates neutralized by positively charged groups on HU are similar for all three modes. The results provide the basis for proposals and tests of model structures for the complexes between HU and DNA in these binding modes.

Background on Coulombic salt effects and on Coulombic end effects

In the salt concentration range investigated here (0.06 M – 0.15 M), effects of NaCl on the binding constant (or standard free energy change) of a nonspecific protein-DNA interaction are proposed to be primarily Coulombic (and therefore primarily entropic effects in water) [30; 31; 32]. No large net contribution to K_{obs} or $\Delta G_{obs}°$ from non-Coulombic (Hofmeister, osmotic) effects of NaCl are expected [33]. Coulombic salt effects are typically manifested as a large negative SK_{obs} (i.e., $\partial \ln K_{obs}/\partial \ln[salt]$) at low salt concentration and originate primarily from the reduction in the local salt cation (counterion) gradient near DNA phosphates (i.e., cation release) upon neutralization of these phosphates by binding of a cationic ligand or a cationic surface of a protein (the polyelectrolyte effect) [34; 35; 36; 37; 38]. Analysis of the Coulombic salt effect provides an estimate of the number of DNA phosphates in the interface and the effective net valence of the DNA binding site of a ligand or protein [34; 35; 37; 39; 40; 41; 42; 43; 44; 45; 46; 47; 48; 49; 50; 51].

Experimental data, nonlinear Poisson-Boltzmann (NLPB) calculations, and Monte Carlo simulations of Coulombic salt effects on nonspecific binding of cationic oligopeptides (L^{z+}) to DNA (or RNA) oligomers have revealed large Coulombic end effects (CEEs), which cause the position-averaged site-binding constant (K_{obs}) and the magnitude of its salt concentration dependence (i.e., $|SK_{obs}|$) to increase strongly with increasing DNA length (up to approximately 40 phosphate charges) at low salt concentration [36; 52; 53; 54; 55; 56]. The CEE decreases in significance with increasing salt concentration, and is typically eliminated above 0.3 M salt. Similar behavior has been observed for nonspecific binding of human DNA polymerase β to single stranded polymeric and 16 nucleotide DNA in the salt concentration range 0.05 – 0.15 M Na^+ with 1 mM Mg^{2+} [28]. Hence a significant CEE on binding of HU to 8 bp and 15 bp DNA (but not 34 bp or larger DNA) is expected in the range of salt concentration investigated here. However, no evidence for a significant CEE was obtained in our previous characterization of the thermodynamics of HU binding to these DNA fragments at 0.15 M Na^+ [10]. Here we obtain circumstantial evidence for a significant CEE from analysis of the salt concentration dependences of the HU-DNA binding constants and explain why our previous experiments did not detect this CEE.

The molecular origin of the CEE which makes K_{obs} and SK_{obs} for DNA binding of a cationic ligand or cationic site on a protein vary with DNA length is the axial dependence of the salt cation concentration gradient surrounding the DNA molecule [36; 56; 57; 58]. In particular, the surface concentration of Na^+, which at low salt concentration (< 0.2 M) greatly exceeds the bulk Na^+ concentration at all locations on DNA, is smaller in the vicinity of the 5 – 6 bp at each end of the molecule than in the interior where it is comparable to the surface Na^+ concentration for interior regions of polymeric DNA. Except at high salt concentration, binding of a cationic ligand or protein at or near the end is disfavored relative to binding to any interior site due to a smaller amount of cation release; the difference in binding constants favoring interior binding increases with decreasing salt concentration because the contribution to the ensemble averaged SK_{obs} from interior binding is more negative than from end binding. Since the fraction of potential nonspecific binding sites for an oligocation or protein which are located within 6 bp of an end decreases with increasing DNA length, the contribution of the CEE to the position-averaged nonspecific site binding constant (and SK_{obs}) decreases with increasing DNA length and is not expected to be significant on 34 bp or longer DNA, as observed for binding of oligocations to DNA [36; 54; 55; 56]. This CEE also explains why an oligocationic ligand or the charges on a typical protein binding site do not contribute nearly as much to the SK_{obs} of DNA binding as do the similar number of DNA phosphates in the polymeric interior of DNA [30]. Predictions of the CEE are obtained from the analytical oligocation model (referred to hereafter as the model CEE case) [56] and from numerical NLPB calculations on structural models of reactants and complexes (see the Discussion).

Results and Analysis

Qualitative features of ITC titrations of various lengths of DNA (8 bp – 160 bp) with HU: persistence of the three DNA binding modes of HU at all salt concentrations examined

The [HU]/[DNA] and DNA length dependences of nonspecific binding of HU to various lengths of DNA observed in ITC titrations have demonstrated the existence of three DNA binding modes of HU and [HU]/[DNA] driven transitions between them at 0.15 M Na^+ [10]. Titrations at lower salt concentrations provide strong evidence for the persistence of all three binding modes of HU at all salt concentrations examined. Previous DSC and CD thermal scans of *E.coli* $HU_{\alpha\beta}$ have demonstrated that unfolding of HU ($\alpha\beta \rightarrow I \rightarrow \alpha + \beta$ where I is a dimeric unfolding intermediate) does not occur until 25 °C in the salt concentration range 0.2 M to 1.0 M Na^+ [59]. Extension of these DSC and CD experiments to the lower salt concentration range of the DNA binding experiments reported here demonstrates that HU remains a stable folded dimer at 15 °C. At or above 25 °C, folding of HU is coupled to binding, affecting the observed binding constant, enthalpy, and heat capacity change (Koh *et al.*, in preparation) [60].

Figure 1a shows the biphasic binding isotherms obtained in titrations of 15 bp DNA with HU at [Na^+] from 0.06 M to 0.125 M, similar to that reported previously at 0.15 M Na^+, but very different from the monophasic 1:1 binding isotherms obtained on 8 bp DNA at all [Na^+] [10] (see Sfig. 1). As [Na^+] is reduced the transition from endothermic to exothermic binding becomes steeper and occurs at lower [HU]/[DNA] (from [HU]/[DNA] = 1.3 at 0.15 M Na^+ to 0.7 at 0.06 M Na^+). The depth of the exothermic minimum increases from – 0.7 kcal/mol at 0.15 M Na^+ to – 3.5 kcal/mol at 0.06 M Na^+. The final phase of the isotherm, in which the heat signal decays to baseline, is also steeper at lower salt concentration, with a distinct inflection point at [HU]/[DNA] ~ 2 (Fig. 1a). These biphasic binding isotherms of 15 bp DNA indicate a binding mode transition as a function of [HU]/[DNA] at all salt concentrations examined here, as observed previously at 0.15 M Na^+ [10]. Initially, for [HU]/[DNA] < 1, HU binds noncooperatively in the endothermic 10 bp mode. Higher [HU]/[DNA] drives the binding mode transition to the cooperative, exothermic 6 bp mode [10]. The

traces of the electrical power, which represents the heat evolved or absorbed for each injection of HU as a function of time, show the complete return of the signal to the baseline over [HU]/[DNA] and the salt concentration range examined, indicating that the kinetics of binding of HU to 15 bp DNA in the two modes and the transition between them are rapid on the time scale of the ITC injections (Sfig. 2). The quantitative analysis in subsequent sections shows that the more abrupt and larger amplitude features of the isotherms at lower [Na^+] are the consequence of large increases in binding constants of both 10 bp and 6 bp modes as [Na^+] is reduced.

Quantitative analysis of these binding isotherms involves six microscopic thermodynamic quantities: site binding enthalpies Δh_{10} and Δh_6, position-averaged site binding constants k_{10} and k_6, cooperativity ω_6, and cooperativity enthalpy $\Delta h\ \omega_6$[10]. As defined previously [10; 61; 62], these microscopic binding constants and enthalpies refer to the binding of HU in binding mode i (occupying n_i base pairs) to one of the $N - n_i + 1$ potential sites on a N bp DNA oligomer. (The quantity $N - n_i + 1$ is called the statistical factor.) The cooperativity ω_6 is defined as the ratio of binding constants for adjacent binding and isolated binding of HU in the 6 bp mode. These six quantities cannot all be determined by fitting the 15 bp DNA binding isotherms. Independent information regarding Δh_6 and k_6 for the 6 bp mode is required and available from titrations of 8 bp DNA with HU (Sfig. 1). While Δh_6 is expected to be independent of DNA length, k_6 is expected to increase with increasing DNA length because of the Coulombic end effect.

At 0.15 M Na^+ and low [HU]/[DNA] (< 1), HU binds 34 bp and longer (38 bp and 160 bp) DNA primarily in the endothermic noncooperative 34 bp mode [10]. An increase in DNA length from 34 bp to 38 bp or 160 bp at low [HU]/[DNA] favors the 34 bp mode relative to the two small site size modes because the statistical factor (i.e., the number of ways that one HU can bind in a particular binding mode to an unoccupied DNA oligomer, defined above) of the 34 bp mode increases much more (relative to its value on 34 bp DNA) than those of the small site size modes as the DNA length increases in this range [10]. As a consequence, the initial heat of binding (i.e., the enthalpy change for formation of an ensemble of 1:1 complexes in the three modes (see Eq. 1 below)), increases as DNA length increases from 34 bp, approaching the binding enthalpy of the 34 bp mode at a DNA length of 160 bp. Figure 1b and c show that very similar DNA length dependences of the initial heat of binding are observed at lower salt concentrations (0.06 M – 0.125 M Na^+), indicating the existence of all three DNA binding modes of HU at all [Na^+] examined. At each [Na^+], the initial heat of binding increases dramatically with increasing DNA length from 34 bp to 38 bp, and then increases only slightly for 160 bp DNA. For each DNA length, the initial heat of binding increases slightly with increasing [Na^+].

Quantitative analysis of the observed DNA length (34 bp, 38 bp, and 160 bp) dependence of the initial heat of binding involves site binding enthalpies (Δh_{34}, Δh_{10}, and Δh_6) and position-averaged site binding constants (k_{34}, k_{10}, and k_6) of the three binding modes [10]. The binding constants and enthalpies of the 10 bp and the 6 bp modes are available from titrations of 8 bp and 15 bp DNA with HU. Here the binding enthalpies of the two modes are expected to be independent of DNA length, while the binding constants are expected to be larger on 34 bp (and larger) DNA than on 8 bp or 15 bp DNA. The CEE is not expected to significantly affect position-averaged nonspecific binding constants for 34 bp and larger DNA, as discussed above.

At 0.15 M Na^+, the ITC isotherm observed in a forward titration of 34 bp DNA with HU is biphasic, exhibiting a transition from endothermic to exothermic binding with increasing [HU]/[DNA] [10]. Analysis of the isotherm reveals that as [HU]/[DNA] increases the binding mode switches from the 34 bp mode to the less endothermic 10 bp mode and the exothermic

6 bp mode, both of which are moderately cooperative [10]. Figure 1d shows that these features become more pronounced as $[Na^+]$ is reduced, indicating that the transitions between the three binding modes as a function of [HU]/[DNA] persist at all salt concentrations examined. The transition from endothermic to exothermic binding heat shifts to lower [HU]/[DNA], becomes steeper, and exhibits a sharper exothermic minimum with decreasing salt concentration, as observed for 15 bp DNA binding isotherms. While the binding isotherms at $[Na^+] \geq 0.125$ M subsequently exhibit decay of the heat signal to the baseline, the isotherms at lower salt concentrations exhibit a second transition prior to decay to the baseline, reverting to endothermic binding with a distinctive inflection point at [HU]/[DNA] ~ 3.5 (Fig. 1d). As observed in 15 bp DNA binding isotherms, the traces of the electrical power as a function of time indicate that the kinetics of binding of HU to 34 bp DNA in the three modes and transitions between them are rapid on the time scale of the ITC injections (Sfig. 2). Our quantitative analysis of these complex features of the 34 bp DNA binding isotherms reveals significant contributions from cooperativity enthalpies of the two small modes to the observed binding heat (see below for further discussion).

Effects of $[Na^+]$ on binding of HU to 8 bp DNA in the 6 bp mode are analogous to those on binding of an octacation (L^{8+}) to a similar DNA oligomer

Microscopic binding constants and enthalpies for the 6 bp mode on 8 bp DNA (k_6, $\Delta h_6°$) obtained from fitting the previous ITC titration data [10] (Sfig. 1) to the 1:1 binding model (Eq. 2, 3) in the salt concentration range 0.06 M to 0.125 M Na^+ are presented in Table 1 together with previously published k_6 and $\Delta h_6°$ at 0.15 M Na^+ [10]. At 15 °C, for all salt concentrations examined, the primary thermodynamic driving force for binding of HU to 8 bp DNA in the 6 bp mode is the positive entropy change even though the enthalpy change is also favorable and significant. Reduction in $[Na^+]$ from 0.15 M to 0.06 M increases k_6 by almost two orders of magnitude (from 3.4×10^4 M^{-1} to 2.7×10^6 M^{-1}): the log-log salt concentration derivative of k_6, $Sk_6 = (\partial \ln k_6/\partial \ln[Na^+]) = -4.9 \pm 0.3$ (Fig. 2a and Table 5). Values of Sk_6 are expected to be more negative (larger in magnitude) on larger DNA as a result of the CEE (see above). A reduction in $[Na^+]$ from 0.15 M to 0.06 M increases the favorable entropic contribution to binding ($T\Delta s_6°$) from 4.4 kcal/mol to 6.4 kcal/mol and makes the binding enthalpy $\Delta h_6°$ slightly more exothermic (from – 1.6 kcal/mol to – 2.1 kcal/mol) (Table 1); $\Delta h_6°$ extrapolates linearly to – 2.3 kcal/mol at the low salt limit (Fig. 2b).

These thermodynamic aspects of binding of HU in the 6 bp mode to 8 bp duplex DNA (14 phosphate charges) are analogous to those of binding of an octacation L^{8+} (KWK_6) to single stranded nucleic acid oligomers with 14 phosphate charges, for which $SK_{obs} = -4.8 \pm 0.3$ [55]. In general, binding of oligocations (L^{z+}) to single- or double-stranded nucleic acids is entropically driven at low salt concentration; this entropic driving force (the polyelectrolyte effect) increases as the salt concentration is reduced [35; 41; 42; 43]. Extrapolated binding free energies at 1 M salt (a useful but hypothetical reference state) are typically small in magnitude (close to zero [35; 41; 42; 43; 55]) as we observe for binding of HU to 8 bp DNA in the 6 bp mode ($\Delta g_6°$ (1 M) = − 0.6 ± 0.3 kcal/mol). The binding enthalpy of the 6 bp mode (approximately – 2 kcal/mol, typically insensitive to salt concentration) is also comparable to $\Delta H_{obs}°$ for L^{z+} – nucleic acid interactions: for interaction of $(Lys)_5CO_2$ with T7 DNA, $\Delta H_{obs}° = -1.3 \pm 0.7$ kcal/mol [39] and for interaction of $(Lys)_5(Trp)_{1\sim3}NH_2$ with poly(U), $\Delta H_{obs}° = -2.0 \pm 1.5$ kcal/mol after correction for the Trp interaction enthalpy [41].

Binding of HU to 15 bp DNA: $[Na^+]$ dependent thermodynamics of the 10 bp mode and competition between the 10 bp and the 6 bp modes

Statistical thermodynamic analysis [10] of the observed binding isotherms of 15 bp DNA, using the binding enthalpy (Δh_6) and a range of possible values of the position-averaged

binding constant (k_6) of the 6 bp mode on 15 bp DNA as inputs to Eq. 2 and 4, yields the binding enthalpy (Δh_{10}) and the corresponding range of the binding constant (k_{10}) of the 10 bp mode at each salt concentration (Table 2). The fit also yields the cooperativity enthalpy ($\Delta h_{\omega 6}$) and the corresponding range of the cooperativity factor (ω_6) of the 6 bp mode (cooperativity factors involving the 10 bp mode (ω_{10} and $\omega_{10/6}$) are quantified from analysis of the 34 bp DNA binding isotherms, given below). Initially, the values of k_6 determined from titrations of 8 bp DNA were used in analysis of HU binding isotherms for 15 bp DNA, as done previously at 0.15 M Na^+ [10] Although excellent fits at all salt concentrations investigated here are obtained using these values of k_6 (Fig. 1a), we subsequently found that equally good fits to the 15 bp DNA binding isotherms were obtained using a range of larger values of k_6 as inputs (Fig. 3). While only a small range of values of k_6 (approximately two-fold) yields acceptable fits to 15 bp DNA binding isotherms at 0.15 M Na^+, a much larger range of k_6 (approximately twenty-fold) is consistent with isotherms at 0.06 M Na^+ (black curves in Fig. 3). These ranges (maximum acceptable values) of the ratio $k_{6,15\text{ bp DNA}}$ / $k_{6,8\text{ bp DNA}}$ are listed in Table 2 for all salt concentrations examined. (Values of $k_{6,15\text{ bp DNA}}$ / $k_{6,8\text{ bp DNA}} < 1$ also provide satisfactory fits but are nonphysical and hence not considered further.) Analyses using values of $k_{6,15bp}/k_{6,8bp}$ greater than the maximum values in Table 2 systematically fail to fit the initial transition from endothermic to exothermic heat signal and the final relaxation to the baseline at all salt concentrations examined (red curves in Fig. 3).

Table 2 reveals that the enthalpies Δh_{10} and $\Delta h_{\omega 6}$ do not change significantly as k_6 is systematically varied, while fitted values of k_{10} increase proportionately at all salt concentrations investigated. For all values of k_6 yielding acceptable fits to 15 bp DNA binding isotherms, the ratio $k_{10}/k_6 = 2.8 \pm 1$. Increasing k_6 causes the best fit value of the cooperativity ω_6 to decrease so that the product $k_6\omega_6$ remains relatively constant within uncertainty at each salt concentration. These correlations of fitting parameters result because for the conditions investigated (relatively high [DNA] and low to moderate [Na^+]), the initial heat of binding (see below) is a function of the ratio k_{10}/k_6 and not the individual values of k_{10} and k_6. In the late stages of the isotherm, binding is mostly in the cooperative 6 bp mode with equilibrium constant $k_6\omega_6$ and therefore if k_6 is increased, the fitted value of ω_6 is reduced to maintain a constant $k_6\omega_6$.

The observation that the ratio k_{10}/k_6 does not vary significantly with [Na^+] or with the choice of $k_{6,15bp}$ used in fitting 15 bp DNA binding isotherms indicates that binding constants of these two modes have the same log-log dependences on [Na^+] (i.e., $Sk_{10} = Sk_6$) on 15 bp DNA. As $k_{6,\ 15bp}$ is increased from $k_{6,8bp}$, Sk_6 on 15 bp DNA decreases (i.e., increases in magnitude) from -4.9 ± 0.3 to -7.4 ± 0.4. As a consequence, k_{10} increases and Sk_{10} decreases (from -4.9 ± 0.3 to -7.2 ± 0.4) on 15 bp DNA. Over the entire range of possible values of $k_{6,15bp}$, Sk_{10} and Sk_6 are the same within the experimental uncertainty (Fig. 4a and Table 5).

For all salt concentrations examined (at 15 °C), the primary thermodynamic driving force for binding of HU to 15 bp DNA in the 10 bp mode is the positive entropy change whereas the enthalpy change is unfavorable. With a reduction in Na^+ concentration from 0.15 M to 0.06 M, the entropic contribution to the binding free energy ($T\Delta s_{10}°$) becomes more favorable (more positive) by 2-3 kcal/mol, while the binding enthalpy (Δh_{10}) becomes less unfavorable (less positive) by about 0.8 kcal/mol (Table 2), extrapolating linearly to ~ 3.0 kcal/mol at the low salt limit (Fig. 4b). Inspection of Table 2 shows that the driving force for the cooperativity of the 6 bp mode is primarily entropic at all salt concentrations investigated.

Population distributions of the 10 bp and the 6 bp (isolated and cooperative) modes on 15 bp DNA at 0.06 M and 0.125 M Na^+ based on the fitting results with $k_{6,15bp}/k_{6,8bp} = 1$ (Table 2) are shown in Figure 5a (other values of $k_{6,15bp}/k_{6,8bp}$ between 1 and the maximum value also yield the similar population distributions at a given salt concentration). Because the ratio of binding constants between the two modes is found to be independent of salt concentration ($k_{10}/k_6 \sim 2.8$), the ratio of populations between the two modes is not strongly affected by changing salt concentration for [HU]/[DNA] < 0.5, the regime where HU forms mostly 1:1 complexes with 15 bp DNA. This result, together with the weak salt concentration dependences of the binding enthalpies of both modes (Table 5), explains the absence of any significant salt concentration dependence of the initial heat of binding. The transition from endothermic to exothermic binding with increasing [HU]/[DNA] (occurring at [HU]/[DNA] = 0.7 at 0.06 M Na^+ and at [HU]/[DNA] = 1.3 at 0.15 M Na^+; see Fig. 1 a) is primarily attributed to replacement of the endothermic 10 bp mode ($\Delta h_{10} \sim +3.5$ kcal/mol) by the exothermic 6 bp mode ($\Delta h_6 = \sim -2.0$ kcal/mol) (Fig. 5b). Increases in the binding constants of the 10 bp and the 6 bp modes with decreasing salt concentration result in a sharper transition from the 10 bp to the 6 bp mode, shifted to lower [HU]/[DNA], at lower salt concentration (Fig. 5a and b). For example, at 0.06 M Na^+, the average number of HU bound in the 10 bp mode per DNA decreases strongly from 0.34 at [HU]/[DNA] = 0.85 to 0.05 at [HU]/[DNA] = 1.7. However, at 0.125 M Na^+, the average number of HU bound in the 10 bp mode is almost invariant (0.34 to 0.32) in the same range of [HU]/[DNA]. The increase in the binding constant of the 6 bp mode also contributes to the steeper decay of the heat signal to the baseline at saturation and to the more pronounced exothermic minimum and the inflection point observed at lower salt concentration.

As reviewed in the Background, the molecular basis for expecting a larger value of k_6 and a more negative Sk_6 for 15 bp DNA than for 8 bp DNA is the Coulombic end effect (CEE). The CEE is expected to be primarily entropic, consistent with the observation that values of Δh_6 from analysis of the 8 bp DNA titrations (Table 1) do not need correction to fit the 15 bp (also 34 bp and larger; see below) DNA binding isotherms. Based on the analogy between binding of HU to 8 bp DNA in the 6 bp mode and binding of L^{8+} to an oligonucleotide with the same number of phosphate charges (see above), HU was modeled as a simple oligocation with a net charge of +8 for theoretical estimation of the CEE on binding of HU to oligomeric DNA in the 6 bp mode. This so-called “model CEE” analysis, previously successfully used to predict the CEE on interactions of oligocations with oligonucleotides [56], is used here to estimate the increase in k_6 on 15 bp DNA as compared to 8 bp DNA at each salt concentration (see Materials and Methods). Predicted ratios $k_{6,15bp}/k_{6,8bp}$ decrease from 21 at 0.06 M Na^+ to 5 at 0.15 M Na^+. Except at 0.06 M Na^+, these predicted values are about two-fold larger than, but the same within uncertainty as, the maximum values of these ratios that provide acceptable fits to the 15 bp DNA binding isotherms. (For example, reducing the length of the end region in the model CEE analysis [56] from 12 to 11 phosphate charges, reduces these predicted ratios by two-fold.)

Binding of HU to 34 bp and longer DNA: analysis of the initial heat of binding as a function of DNA length and salt concentration indicates that the three binding modes of HU have similar salt concentration dependences of binding constants, Sk_i

Analysis of the initial heat of binding of HU to 34 bp and selected larger DNAs provides a direct way to determine the binding enthalpy and the range of possible binding constants for the 34 bp mode, free of contributions from the cooperativities of the 10 bp and the 6 bp modes [10]. Moreover, Coulombic end effects are not significant for interpretation of position-averaged nonspecific HU binding constants for 34 bp or larger DNA (see Background). The analysis of initial binding heats requires that only 1:1 complexes between HU and DNA molecules be present and that the free HU concentration be negligibly small (i.e.,

stoichiometric binding) [10] To achieve this condition, the concentration of DNA in the ITC reaction cell is increased until the initial heat signal reaches a [DNA]-independent plateau for each DNA length (Fig. 1b inset). At the [DNA]-independent plateau, the initial heat of binding for each DNA length (N bp) is given by:

$$Q_{\text{initial,N bp DNA}} = \sum_{i=6,10,34} \Delta h_i \frac{(N - n_i + 1)k_i}{\sum_{i=6.10.34}(N - n_i + 1)k_i} \quad \text{(Eq. 1)}$$

where n_i is the binding site size of the binding mode i and $\frac{(N - n_i + 1)k_i}{\sum_{i=6,10,34}(N - n_i + 1)k_i}$ is the fractional population of the 1:1 complex in the binding mode i [10]. Division of both numerator and denominator by k_6 rearranges Eq. 1 in terms of the ratios k_{34}/k_6 and k_{10}/k_6.

Fits of initial heats of HU binding to 34 bp, 38 bp, and 160 bp DNA to Eq. 1 (Fig. 1 b), using binding enthalpies (Δh_{10}, Δh_6) and binding constant ratios k_{10}/k_6 as inputs, yield the binding enthalpy (Δh_{34}) and relative binding constants (k_{34}/k_6 and k_{34}/k_{10}) of the 34 bp mode as a function of [Na^+]. In this analysis, binding enthalpies for the 10 bp and the 6 bp modes determined from analyses of the 15 bp and the 8 bp DNA binding isotherms (Table 1 and 2) are directly used and ranges of binding constants (therefore k_{10}/k_6) for the two modes derived from various assumptions regarding CEEs are examined. As one limiting case (that specified as “no CEE” in Table 3), we assume that k_6 and k_{10} are independent of DNA length so that values of these quantities determined from analyses of 8 bp and 15 bp DNA titrations neglecting CEEs (from Table 2) are directly applicable to 34 bp and larger DNA. In other analyses, values of k_6 and k_{10} are increased from their values on 15 bp (and 8 bp) DNA given in Table 2. The maximum increase in k_6 from 8 bp to 15 bp DNA at each salt concentration consistent with the ITC results (see Table 2), which is also most consistent with that predicted by the model CEE analysis (see above), was considered as the most plausible case. Likewise, the most plausible increases in k_6 and k_{10} from 15 bp to 34 bp DNA were estimated at each salt concentration based on the model CEE predictions, and are listed in Table 3 (model CEE).

Significantly, Table 3 reveals that the fitted values for ratios of position-averaged site binding constants k_{34}/k_6 (69 ± 12) and k_{34}/k_{10} (21 ± 5), valid for 34 bp and larger DNA, are relatively independent of both [Na^+] and the assumptions about CEE used in the analyses. These results show that the log-log [salt] derivatives of the binding constants (Sk_i) of the three modes are the same within uncertainty, independent of assumptions regarding the magnitudes of k_6 and k_{10} as functions of DNA length. Values of Sk_i for the three modes on 34 bp and longer DNA are − 4.9 ± 0.3, − 4.9 ± 0.3, and − 5.3 ± 0.5 for the 6 bp, the 10 bp, and the 34 bp modes, respectively, if there is no DNA length dependence of k_6 and k_{10} (Fig. 6a and Table 5). If k_6 and k_{10} have the DNA length dependences predicted by the model CEE analysis, more negative Sk_i are obtained: Sk_6 = − 7.5 ± 0.4, Sk_{10} = − 7.4 ± 0.4, and Sk_{34} = − 7.8 ± 0.7 (Fig. 6a and Table 5).

Fitted values of the binding enthalpy Δh_{34} for the bent 34 bp mode are completely insensitive to assumptions about CEE on k_6 and k_{10} used in the analyses and are more endothermic at all salt concentrations than observed for the smaller-site-size modes. For all salt concentrations examined (15 °C), the primary thermodynamic driving force for binding of HU to 34 bp and longer DNA in the 34 bp mode is the positive entropy change whereas the enthalpy change is unfavorable. With a reduction in Na^+ concentration from 0.15 M to 0.06 M, the favorable entropic driving force ($T\Delta s_{34}°$) increases from 16.9 kcal/mol to 21.0 kcal/mol for the model CEE case (Table 3). (Alternatively, if k_6 and k_{10} were assumed to be

independent of DNA length (no CEE), then a somewhat smaller increase in $T\Delta s_{34}°$ is predicted: 16.5 kcal/mol at 0.15 M Na^+ to 19.3 kcal/mol at 0.06 M Na^+.) The binding enthalpy (Δh_{34}) decreases from 7.8 kcal/mol at 0.15 M Na^+ to 6.7 kcal/mol at 0.06 M Na^+, extrapolating linearly to 6.2 kcal/mol at the low salt limit (Fig. 6b). In addition to the two choices described above and listed in Table 3, we examined the entire ranges of DNA length dependent values of k_6 and k_{10} consistent with both initial binding heats and the entire 34 bp DNA binding isotherms and found that the conclusions regarding Δh_{34} and ΔSk_i are not significantly affected (see supplemental information).

[Na^+] effects on the competition between the three binding modes of HU on 34 bp DNA: evidence for exothermic cooperative interactions of HU involving the 10 bp mode (ω_{10}, $\omega_{10/6}$)

The entire 34 bp DNA binding isotherms were analyzed using the modified sequence generation function method (SGF) (Fig. 1d) previously developed to describe the competition between the 34 bp, the 10 bp, and the 6 bp modes on 34 bp DNA (Eq. 5–7) [10]. In this analysis, values of k_{34}, k_{10}, k_6, Δh_{34}, Δh_{10}, Δh_6, ω_6, and $\Delta h_{\omega 6}$ determined from analyses of 8 bp and 15 bp DNA binding isotherms and of initial heats of binding for 34 bp, 38 bp, and 160 bp DNA with different assumptions of CEEs (see above) were used to obtain the cooperativities involving the 10 bp mode (10 bp mode (ω_{10}) and intermode ($\omega_{10/6}$)) and their associated enthalpies ($\Delta h_{\omega 10}$ and $\Delta h_{\omega 10/6}$) (Table 4). Equivalently acceptable fits describing all the features of the binding isotherm were obtained for both the model CEE and the no-CEE cases at each salt concentration (Fig. 1d). At all salt concentrations examined, the increases in k_{10} and k_6 reduce ω_{10} and $\omega_{10/6}$ without significantly affecting values of $\Delta h_{\omega 10}$ and $\Delta h_{\omega 10/6}$ (Table 4), as observed in analysis of 15 bp DNA binding isotherms.

Values of ω_{10} and $\omega_{10/6}$ obtained from analysis of the entire 34 bp DNA binding isotherms are moderate to weak depending on the CEE assumption used in the analysis at all salt concentrations examined (Table 4). The corresponding enthalpies are significantly exothermic for any case at all salt concentrations examined (Table 4) and are primary driving forces for the 10 bp mode and intermode cooperativities, in contrast to the entropically driven and enthalpically unfavorable 6 bp mode cooperativity (Table 2). With decreasing salt concentration from 0.15 M to 0.06 M Na^+, ω_{10} increases ~ 3-fold for the no-CEE case and is more or less constant if the model CEE case is used, whereas $\omega_{10/6}$ does not show a monotonic dependence on salt concentration with the minimum value at 0.125 M Na^+. $\Delta h\ \omega_{10}$ decreases by ~ 4 kcal/mol from 0.15 M to 0.06 M Na^+ whereas $\Delta h\ \omega_{10/6}$ does not show any systematic salt concentration dependence with an average value of ~ − 3.0 kcal/mol.

The exothermic cooperativity enthalpy of the 10 bp mode significantly contributes to the transition from endothermic to exothermic binding heat observed in the first half of 34 bp DNA titrations (Fig. 7c, d) because the population of the contact point between two adjacent HU molecules bound in the 10 bp mode increases cooperatively with increasing [HU]/[DNA] (i.e., positive curvature in the average number of contact points per DNA, Fig. 7a, b). After this transition, the observed binding heat reflects the net conversion of cooperatively bound HU molecules in the 10 bp mode to those in the 6 bp mode (Fig. 7c, d). The endothermic dissociation of cooperative clusters of HU in the 10 bp mode is the primary origin of the endothermic peaks observed at low salt concentrations (Fig, 7a, c). The enthalpy of the intermode cooperativity is important in determining the details of the shape of the exothermic minimum and the endothermic maximum (Fig. 7c, d). All of these features become more pronounced as the salt concentration is reduced, because the increases in binding constants of all modes cause the binding mode transitions to become sharper, as observed for 15 bp DNA binding isotherms. The 34 bp mode contributes to the population

distribution and to the observed binding heat only at low [HU]/[DNA], as observed previously [10].

Discussion

DNA binding mode transitions of *E.coli* $HU_{\alpha\beta}$ as a function of [HU]/[DNA] and DNA length are observed at all salt concentrations examined

ITC studies of nonspecific binding of HU to DNA oligomers at low to moderate salt concentration (0.06 M – 0.15 M Na^+, 15 °C) demonstrate the existence of three (6 bp, 10 bp, 34 bp) binding modes differing in position-averaged, nonspecific site binding constant k_i at a constant salt concentration. Significantly, the binding constant ratios k_{34}/k_{10} and k_{34}/k_6 on 34 bp and longer DNA are found to be independent of salt concentration and of the assumptions made regarding the Coulombic end effect (CEE), within experimental uncertainties. Therefore, the log-log [salt]-derivatives of the binding constants, Sk_i, are the same for all three binding modes on 34 bp and larger DNA within uncertainty.

However, values of Sk_i for the individual modes do depend sensitively on the role assigned to the CEE, because the characterizations of the small site size modes were performed with short DNA oligomers. To unambiguously determine k_i for the 6 bp mode as a function of salt concentration and therefore obtain Sk_i for this mode requires using a DNA shorter than 10 bp to avoid binding of HU in the 10 bp mode. We obtain $Sk_i \sim -5$ for the 6 bp mode on 8 bp DNA; reducing [Na^+] from 0.15 M to 0.06 M increases k_6 by about two orders of magnitude. But the CEE is predicted to be most significant for such short oligomers. If there were no CEE, and Sk_i for the 6 bp mode were – 5 for all DNA lengths, then we would conclude that Sk_i are also – 5 for the 10 bp and the 34 bp modes for all DNA lengths. On the other hand, use of the model CEE analysis yields calculated values of Sk_i of approximately – 8 for all three modes on polymeric DNA (≥ 34 bp).

In this range of salt concentration, binding enthalpies of the three modes are insensitive to the magnitude of the CEE and decrease linearly (i.e., become more exothermic) with decreasing salt concentration. The largest site size (34 bp) mode exhibits the largest dependence of the binding enthalpy on salt concentration.

Because the ratios of the binding constants between different modes are independent of salt concentration, [HU]/[DNA] and DNA length (34 bp to 160 bp) driven binding mode transitions observed previously at 0.15 M Na^+ [10] occur at all other salt concentrations examined in this study. Binding enthalpies of the three modes differ significantly from each other in magnitude at all salt concentrations investigated, allowing the binding mode transitions to be readily detected by ITC. Binding mode transitions driven by the [HU]/[DNA] ratio are the origin of the multiphasic features of the HU binding isotherms for 15 bp and longer DNA (Fig. 1). These features become more pronounced at lower salt concentration because the increases in binding constants of all modes cause sharper transitions between the modes as a function of [HU]/[DNA]. For example, the [HU]/[DNA] ratio where fractional populations of the 10 bp and the 6 bp modes on 34 bp DNA are equal shifts from 11.0 at 0.15 M Na^+ to 3.7 at 0.06 M Na^+ (Fig. 7b and Sfig. 3a). Similar salt concentration dependent features have been reported in a recent single-molecule force extension measurement study [63] where the transition from compaction to stiffening of DNA with increasing HU concentration becomes less pronounced at higher salt concentration.

Salt concentration driven binding mode transitions are observed in interactions between *E.coli* SSB and single stranded DNA as a consequence of the large differences in values of SK_{obs} for the different modes [23; 24; 25], in contrast to the similar SK_{obs} values for all three DNA binding modes of HU. The transition from the 35 nucleotide (nt) mode to the 65 nt

mode on poly(dT) is driven by increasing NaCl concentration with $\Delta SK_{obs,\ transition} = SK_{obs,\ 65} - SK_{obs,35} = +8$, interpreted as the net uptake of ~ 8 salt ions ($6\ Na^+$, $2\ Cl^-$) [25]. A stable complex with the intermediate site size of 56 nt was also observed in this binding mode transition. Because $\Delta SK_{obs,\ transition}$ is large, SSB binds poly(dT) exclusively in the 35 nt mode at low salt concentration ([NaCl] < 0.01 M) and in the 65 nt mode at high salt concentration ([NaCl] < 0.2 M), and exhibits [SSB]/[DNA] dependent transitions between these modes at intermediate salt concentration (0.01 M < [NaCl] > 0.2 M) [64]. Uptake of cations in the transition from the 35 nt to the 65 nt mode is found to be necessary to reduce the charge repulsions caused by bringing phosphate residues in close proximity upon further wrapping of ssDNA (i.e., negative cooperativity within the ssDNA binding sites of SSB), overriding the release of cations from neutralization of additional DNA phosphates by SSB [25; 65; 66].

Binding of scRPA (yeast single stranded DNA binding protein) to poly(dT) was observed to behave similarly to SSB [27]. At low salt concentration ([NaCl] < 0.1 M), scRPA utilizes the 19 nt mode in the interaction with poly(dT) whereas the 27 nt mode is the dominant mode at high salt concentration ([NaCl] > 1 M). Human DNA polymerase β exhibits 16 nt and 5 nt binding modes for ssDNA at all salt concentrations examined [28], but the appreciable difference in SK_{obs} between the two modes ($\Delta SK_{obs} \sim 3$) predicts that only single binding mode may be observed at sufficiently low or high salt concentration.

The presence of multiple binding modes and transitions between them may be general features for nonspecific single or double stranded DNA binding proteins including IHF (Koh *et al*., in preparation) [60], other NAPs, and the nucleosome. Indeed, the nucleosome has been observed to be dynamic in terms of the extent of wrapping of DNA on its surface, populating at least two different conformations, wrapped and partially unwrapped forms [67; 68; 69]. These different modes have been proposed to be important for regulatory proteins to gain access to their target DNA sequences in the nucleosome [67; 68; 69]. Equilibrium constants for partial unwrapping were recently determined by FRET, and range from ~ 0.02 to ~ 0.1 in the salt concentration range 0.1 M to 0.15 M [68]. For converting the bent (but not wrapped) 34 bp mode to the unbent 10 bp mode of binding of HU, we find $k_{10}/k_{34} = 0.05$ (Table 3), comparable to these nucleosome results.

Interpretation of Sk_i for formation of the DNA binding modes of HU: DNA in the 34 bp mode is bent, but not wrapped, around the α–helical body region of HU

It is remarkable that the observed salt concentration dependences (Sk_i) of binding constants of the three DNA binding modes of HU are similar, given the large differences in the binding site sizes between these modes. What insight does this observation provide regarding the structures of these modes and molecular processes involved in the transitions between them? Sk_i may be interpreted in terms of a long-range Coulombic salt effect; the net Hofmeister-osmotic contribution to Sk_i should be minimal because all the titrations were performed at low to moderate concentration of NaCl [32; 33] and because the extent of dehydration of HU and DNA upon binding in these three nonspecific modes appears to be small (see below for discussion of salt concentration dependences of binding enthalpies) [32; 70; 71]. Therefore, the net charge on the DNA binding interface of HU is expected to be a key determinant of Sk_i. Here, we propose model structures for the complexes between HU and DNA in the three binding modes based on the thermodynamic observations, analyze distributions of charged residues in their binding interfaces, and finally examine Coulombic salt effects on stabilities of these model structures by NLPB calculations.

A structural model of the HU-DNA 34 bp binding mode—The similar values of Sk_i observed for the three binding modes of HU most simply indicate that the charge-charge interactions and the extent of salt ion release in formation of the binding interfaces for these modes are similar. Therefore, bending of DNA and consequent additional interactions that distinguish the bent 34 bp mode from the unbent 6 bp and 10 bp modes must increase the steric binding site size greatly without increasing the number of charge-charge interactions and the extent of salt ion release. The FRET-determined DNA bend angle in the 34 bp mode complex is ~ 140° [10]. This bend angle, which is similar to that observed in the crystal structure of the complex between *Anabaena* HU (AHU) and a mismatched duplex DNA [21], must be large enough to bring the 5′ and 3′ terminal flanking regions of 34 bp DNA sufficiently close to the α – helical body region of HU to prevent binding of another HU molecule. However, this bend angle is not as large as that observed for the IHF – H′ DNA specific complex [32; 72] which allows tight wrapping of the flanking DNA regions on the body of the protein and formation of additional charge-charge interactions. Therefore, the experimentally-determined Sk_i for the formation of the 34 bp mode must result primarily from the salt ion release that accompanies formation of the binding interface between DNA and the HU β – arm/saddle region which is also thought to be the binding interface of the 10 bp mode [6; 14; 16; 22].

To model the 34 bp binding mode complex formed by *E.coli* HU (EHU) and 34 bp DNA, we began with the crystal structure of the AHU-DNA complex [21] (Fig. 8a). The short (17mer) mismatched DNA oligomer in that structure was replaced by the bent 34 bp duplex DNA from the crystal structure of the IHF – H′ DNA complex (in which the DNA is nicked at one proline insertion site) [72]. The overall bend angle of the DNA was reduced from 163° (IHF) to 140° (HU) (Fig. 8b). AHU amino acid side chains were converted to those of EHU as described in Materials and Methods.

Figure 8c and d summarize the numbers of positively and negatively charged residues of HU as a function of distance (from 3 Å to 10 Å) from the nearest anionic DNA phosphate oxygen in this model of the HU-DNA 34 bp mode. The net charge (i.e., the difference between the numbers of cationic and anionic residues) on the DNA binding interface of HU increases from +3 to +10 as the distance defining the contact interface in the complex is increased from 3 to 8 Å. Additional increase in this distance from 8 to 10 Å causes the net charge to decrease from +10 to +9 because there are more anionic residues than cationic residues at this distance range. Significantly, for any distance defining the contact interface, most of the interactions between charged residues of HU and DNA phosphates are located in the interface formed between the central 10 bp region of DNA and the β – arm/saddle region of HU, making at least 80 % contribution to the net charge on the DNA binding interface (Fig. 8c). This center biased distribution of the net charge is consistent with our proposal that salt ion release (primarily Na^+ release from the DNA) in forming the 34 bp mode HU-DNA complex occurs primarily in the binding interface formed by the arm/saddle region of HU since DNA is bent toward, but not wrapped on, the body of HU. (See below for further discussion of the charged residues of HU in the DNA binding interface.)

Recent studies of relaxation kinetics of the IHF – H′ DNA complex perturbed by laser induced temperature jump showed that the forward rate constant for the step where a specific but unbent complex converts into a final specific IHF – DNA complex through bending and subsequent wrapping of DNA does not depend on salt concentration [73] Based on this observation, it was proposed that there is no salt ion release in the formation of the transition state in which DNA is bent, but not yet wrapped on the α – helical body region of IHF. The 34 bp mode of HU observed in our ITC studies may therefore resemble the transition state of the IHF-DNA complex observed in the DNA bending/wrapping step.

A structural model of the HU-DNA 10 bp binding mode—The interface formed between the β – saddle/arm region of HU and the central region of DNA observed in the crystal structure (Fig. 8a) (and in the proposed model of the 34 bp mode (Fig. 8b)) spans ~ 10 bp and has been proposed to be the binding interface of the 10 bp mode [6; 14; 16; 22]. Because the DNA bound in the 10 bp mode is unbent, the conformations of the HU arms must differ in the 10 bp and the 34 bp modes. Indeed, substituting a linear 34 bp DNA for the bent 34 bp DNA in the model structure of the 34 bp mode (Fig. 9a) results in significant steric clash between the arm of HU and the DNA phosphate backbone/bases (purple circle in the foreground of fig. 9a). For this model, the binding site size defined by the arms is approximately 14 bp, not 10 bp. [The origin of the clash is the narrower minor groove for the linear duplex DNA than for the bent DNA near the bending point.] NMR spectroscopy studies revealed that the arms of free *Bst* HU (residues 55 to 74), each of which consists of two β strands and an intervening loop, are highly flexible, populating multiple conformations [74; 75]. The pair of highly conserved alanine residues at 57 and 73 serves as a hinge between the flexible arm and the rigid body/saddle region [74; 76; 77]. The observed flexibility of the arms, which is consistent with the absence of electron density for these regions in crystal structures of free HU [22; 59; 76; 78], indicates that the arms may readily change their conformations in the transition between the different binding modes.

Figure 9a illustrates one plausible conformation of the flexible arm in the 10 bp mode (purple arrow) that minimizes steric clash with the phosphate backbone and bases of unbent DNA; this conformation displays a binding site size of approximately 10 bp. In this model of the 10 bp mode, the tips (the intervening loops) of the HU arms are pulled out of DNA minor groove. As a consequence, the two proline “levers” (green sticks in the 34 bp mode model) are not inserted into DNA base-pairs, which is compatible with the unbent DNA conformation. Most of the interface involving the arm/saddle of HU and the central region of DNA is conserved between the model structures of the 34 bp and the 10 bp modes (Fig. 9a). Therefore, at any contact distance the net charge on the DNA binding interface of HU is similar for these two models (Fig. 9c).

A structural model of the HU-DNA 6 bp binding mode—The simplest interpretation of the similar values of Sk_i for the 6 bp mode and the other two larger modes is that the charged region of the arm/saddle of HU is also the primary DNA binding interface for the 6 bp mode, possibly in a different orientation from that observed in the other two modes. For example, rotating the HU molecule in the model structure of the 10 bp mode around the axis perpendicular to the DNA helical axis by ~ 50° reduces the binding site size from 10 bp to 6 bp (Fig. 9b). The net charge on the DNA binding interface at any distance in this model structure is similar to those obtained for the 34 bp and the 10 bp modes (Fig. 9c). Alternatively, or in addition, conformational changes in the HU arms may occur in the conversion from the 10 bp to the 6 bp mode as a means of reducing the binding site size while maintaining the relative orientation of HU and the primary binding interface observed in the 34 bp and the 10 bp modes.

Possibly the similarity between values of Sk_i for the 6 bp mode and the larger modes on polymeric DNA is only a coincidence and does not imply that the same region of the saddle and arms is the binding site; the binding site for DNA could be on the body of HU. However, there is no evidence for such an interpretation, and several arguments against it. All the binding isotherms on 15 bp and larger DNA obtained in this study are well interpreted in terms of competition between these three modes for binding to DNA; such competition is most simply explained if all three modes utilize similar binding surfaces of HU. In particular, experiments in DNA excess provide no evidence for a binding stoichiometry of 1 HU:2 DNA, as would be expected if the site for the 6 bp mode were distinct from that of the 10 bp and 34 bp modes. Moreover, no other region on the surface of

HU has a local excess of cationic side chains similar to that of the site in the saddle/arm for the 34 bp and 10 bp modes. In particular, the flanking regions on the body of HU, used by IHF to wrap DNA in its specific 34 bp mode, are not sufficiently positively charged to be a binding site, and indeed do not contact DNA in the bent but not wrapped 34 bp mode of HU. Further structural and thermodynamic studies are required to establish a complete model for the 6 bp mode.

The different orientations of the bound HU molecule proposed for the 10 bp and the 6 bp modes indicate that the cooperative HU-HU interactions on DNA must occur through different regions of HU in the two modes. Remarkably different thermodynamic origins of the cooperativities for the two modes (ω_{10} vs. ω_6) support this hypothesis (Table 2 and 4): cooperative interactions between two adjacent HU molecules bound in the 10 bp mode are enthalpically driven at all salt concentrations examined whereas cooperative interactions for the 6 bp mode are entropically driven. Moreover, $\Delta h_{\omega 10}$ becomes more exothermic with decreasing salt concentration while $\Delta h_{\omega 6}$ becomes more endothermic. A conserved hydrophobic patch centered on residue 45V (or I) in the turn between β strand 1 and 2 was previously proposed to be a putative protein-protein interaction surface [22; 77]. This patch is located on the "side" (yellow circles in fig. 9a) of the HU molecule where contact points may readily form between adjacent HU molecules bound in the 10 bp mode.

Nonlinear Poisson – Boltzmann (NLPB) calculations using the structural models to interpret experimental salt concentration dependences of the binding constants (Sk_i) for the three DNA binding modes of HU—The similar distributions of the net charge on the binding interface for the model structures of the three DNA binding modes of EHU are consistent with the similar Sk_i of the three modes determined from analysis of ITC data. To test these structural models further, we performed all-atom nonlinear Poisson – Boltzmann (NLPB) analysis [79] of salt concentration dependences of Coulombic free energy changes for formation of the model complexes (see Materials and Methods for details). NLPB calculations of Coulombic free energies of HU, DNA oligomers, and their complexes in each binding mode as a function of salt concentration yield the thermodynamic extents of salt ion accumulation for these components (n_{HU}, n_{DNA}, $n_{complex}$). The difference ($n_{complex} - n_{HU} - n_{DNA}$) yields the predicted value of Sk_{NLPB}. For a given DNA length, we find that NLPB-predicted values of Sk_{NLPB} for all three binding modes are the same within ~ 10 %, and also the same as those obtained from analysis of ITC data using the model CEE case (Table 5). For binding to 15 bp DNA, we find that Sk_{NLPB} = -7.1 and -7.5 for the 6 bp and the 10 bp modes, respectively. For binding to unbent 34 bp DNA, we find that Sk_{NLPB} = -7.3, -8.2, and -8.3 for the 6 bp, the 10 bp, and the 34 bp modes, respectively. The calculated Sk_{NLPB} for binding of HU to a pre-bent DNA to form the 34 bp mode complex (with no additional DNA bending) is -8.9; the calculated Sk_{NLPB} for bending 34 bp of initially-linear DNA by ~ 140° is + 0.6, yielding Sk_{NLPB} = -8.3 for forming the bent 34 bp complex from HU and linear 34 bp DNA. [The small positive value of Sk_{NLPB} which we calculate for DNA bending indicates that charge repulsions caused by bringing DNA phosphates closer to each other at the narrowed central minor groove and at the underside of the proline insertion site do not contribute significantly to Sk_{34}.]

The value of $Sk_{6,\ NLPB}$ for 8 bp DNA (-5.7), which is comparable to the ITC-determined value (-4.9), demonstrates a very significant Coulombic end effect for the 6 bp mode as compared to $Sk_{6,\ NLPB}$ for 15 bp DNA. Both $Sk_{6,\ NLPB}$ and $Sk_{10,\ NLPB}$ are predicted to change only slightly with increasing DNA length from 15 bp to 34 bp DNA (see above). Hence, position-averaged values of Sk_{NLPB} calculated for the 6 bp and the 10 bp modes on 15 bp DNA are close to the polymeric (≥ 34 bp) limit; the CEE is predicted by NLPB analysis to be of great significance only for binding of HU to 8 bp DNA.

The effective net charges ($Z_{L,eff}$) on the binding interfaces of the three modes were estimated using the values of Sk_{NLPB} on 34 bp DNA (i.e., polymeric Sk_{NLPB}) and the relation, Skpolymeric = – 0.89$Z_{L,eff}$, from the charged cylindrical DNA – oligocation binding model [34; 35; 36; 39] The estimated values of $Z_{L,eff}$ are +8, +9, and +10 for the 6 bp, the 10 bp, and the 34 bp modes, respectively, which are consistent with the net charges calculated from the numbers of the charged residues of HU within 8 Å of DNA phosphates in the model complexes (Fig. 9c). [For estimation of $Z_{L,eff}$ for the 34 bp mode, the value of Sk_{34}, NLPB before the correction for the effect of salt concentration on DNA bending (Sk_{34}, NLPB = – 8.9) was used.] There are 13 cationic residues (αK51, αR55, αR58, αR61, αK83, αK86, βK53, βR55, βR58, βR61, βR80, βK83, βK86) and 3 anionic residues (αE57, αE68, βE68) in the 8 Å-defined DNA binding interface of the 34 bp mode (Fig. 8b, d). All these residues except αK83 and βK83 are located in the interface formed between the central 10 bp region of DNA and the arm/saddle region of HU. In the 10 bp mode, unbending of DNA removes αK83 and βK83 from the 8 Å-defined binding interface while the conformational change of the HU arm removes α/βR61, αE57, and βE68 from this interface but adds an additional cationic residue αK67 (Δnet $charge_{34\rightarrow 10bp\ mode}$ = -1). From the 10 bp mode to the 6 bp mode, rotating the bound HU molecule removes αK67, αK86, and αE68 from the binding interface (Δnet $charge_{10\rightarrow 6_{bp\ mode}}$ = -1). Many of the charged residues of EHU found in the 8 Å-defined DNA binding interfaces of the model complexes are also present in the binding interface for the crystal structure of the AHU-mismatched 17 bp DNA complex (Fig. 8a: αR55, αR58, αR61, αR86, βR53, βR55, βR58, βR61, βR86).

Four cationic residues in the proposed binding interfaces (R55, R58, R61, and R or K86) are highly conserved in HU homologues from different organisms and have been proposed and shown to play important roles in DNA binding [22; 75; 76; 80; 81; 82; 83]. For example, mutation of either R55, 58, or 61 into glutamate significantly reduced (3 to 7-fold in filter binding assays) the apparent DNA binding constant of the wild type *Bst* HU whereas conservative mutation into lysine did not have any significant effect [82]. *E.coli* HU with mutations of R58 and R61 into glycines was also observed to be eluted at lower salt concentration than the wild type in DNA affinity chromatography [83].

Interpretation of salt concentration dependences of $\Delta H_{obs}°$ for formation of the DNA binding modes of HU

For two large-interface protein-DNA complexes in which DNA is wrapped on the protein surface, binding enthalpies increase with increasing salt concentration, strongly in $Cl^-$and Br^- salts, and modestly in F^- and Glutamate salts [32; 84; 85; 86; 87] At 25 °C, the binding enthalpy of SSB in the 65 nt mode to one $(dT)_{70}$ or two $(dT)_{35}$ increases from − 150 kcal/mol at low salt concentrations of NaCl or NaBr (< 0.1 M) to − 94 kcal/mol at 2.0 M NaCl and to −70 kcal/mol at 2.0 M NaBr but is unaffected by increasing concentration of NaF up to 0.6 M [84] For the specific complex of IHF with H′ DNA, in which 34 bps are wrapped around the protein [72], $\Delta H_{obs}°$ at 20 °C increases from − 20 kcal/mol at 0.04 M KCl to − 9 kcal/mol at 0.33 M KCl and from − 22 kcal/mol at 0.04 M KF to − 17 kcal/mol at 0.38 M KF [32] For IHF binding to H′ DNA, $\Delta H_{obs}°$ is a linear function of salt concentration ($\partial\Delta H_{obs}°/\partial$[MCl] = 38 kcal/mol/M), as expected for a Hofmeister effect, and the positive slope is attributed to disruption of weak, enthalpically favorable Hofmeister interaction of Cl^- anions (and to a lesser extent F^- and Glu^- anions) with the surface on the free protein that is buried in the interface of the complex [32] Therefore, the magnitude of salt concentration dependence of $\Delta H_{obs}°$ is proportional to the amount of surface area buried (ΔASA) in complexation.

The situation is quite different for HU. Binding enthalpies of all three DNA binding modes of HU in NaCl increase modestly with increasing [NaCl] (Table 5), with slopes of ~ 11.2, 7.6 and 5.4 for the 34 bp, the 10 bp and the 6 bp modes, respectively. The ΔASA for the

model structure of the HU 34 bp mode is only half as large in magnitude as for the IHF – H′ DNA complex (-2880 Å^2 vs. -5340 Å^2) due to the absence of tight wrapping of the flanking DNA regions on the body of HU. Since values of $\partial\Delta H_{obs}°/\partial[MCl]$ for IHF and HU binding differ by more than three-fold, it is likely that there is also less dehydration per A^2 of surface buried in forming the nonspecific HU-34 bp DNA complex than in forming the specific IHF-34 bp H′ DNA complex. The ratio of $\partial\Delta H_{obs}°/\partial[MCl]$ values comparing the 34 bp and the 10 bp modes of HU (~ 1.5) is comparable to the ratio of ΔASA calculated from the corresponding model structures (2880Å^2 / 1840Å^2 ~ 1.6), but significantly smaller than the ratio of the binding site sizes of the two modes (3.4), consistent with the absence of tight wrapping of the flanking DNA regions around the body of HU in the 34 bp mode.

The more positive binding enthalpy of the 34 bp mode as compared to the 10 bp mode in the salt concentration range examined here (and extrapolated to 0 M salt) may reflect the net effect of the interactions involved in bending the DNA by the HU "machinery": loss of base stacking ($\Delta H° > 0$) [88; 89], gain of interactions between unstacked bases and the proline ($\Delta H° < 0$), and release of ordered water molecules from the DNA minor groove upon burial of the tip of the HU arm containing the proline ($\Delta H° > 0$) [90]. The moderately endothermic binding enthalpy of the 10 bp mode may be also attributed to release of ordered water molecule from the DNA minor groove interacting with the saddle and the lower arm regions. Molecular interpretation of the binding enthalpy of the 6 bp mode (and unambiguous dissection of Δh_{34} and Δh_{10}) requires further structural and thermodynamic characterizations.

Conclusion

Using salt concentration as a probe, we examined the thermodynamic basis of stabilities and the characteristics of the HU-DNA interfaces for the 34 bp, the 10 bp, and the 6 bp binding modes by ITC. All three modes are significant at all salt concentrations examined and exhibit very similar dependences of their stabilities ($\Delta g_i°$) on salt concentration (similar values of $d\Delta g_i°/d\ln[salt] = -RT\,Sk_i$). As a consequence, binding mode transitions driven by changes in [HU]/[DNA] ratio and in DNA length occur at all salt concentrations examined. Our comprehensive analyses of ITC data for different lengths of DNA also provide circumstantial evidence for Coulombic end effects on binding of HU to short DNA oligomers (≥ 15 bp). The similar values of Sk_i for the 6 bp, the 10 bp and the 34 bp modes indicate that the binding interfaces in these complexes involve similar numbers of charge-charge interactions and that the DNA flanking the central 10 bp region which interacts with the saddle and arms of HU is bent toward, but not wrapped on, the body of HU. This structural proposal is corroborated by the observation that the ratio of values of $\partial\Delta H_{obs}°/\partial[MX]$ for the 34 bp and 10 bp modes is smaller than the site size ratio and that $\partial\Delta H_{obs}°/\partial[MX]$ for the 34 bp mode is much smaller than that of the tightly wrapped H′ DNA -IHF complex [32] [The difference in the extent of DNA bending between HU and IHF also results in strikingly different temperature dependences of the binding enthalpies for these two proteins (Koh *et al.*, in preparation) [60].]

The relatively weak binding constant (at ~ 0.15 M Na^+) and the absence of tight wrapping of DNA in the 34 bp mode complex presumably mean that DNA bending by this mode is rapidly reversible, consistent with the lack of detectible kinetics in the ITC titrations and with the observation of a greatly reduced persistence length (stiffness) of DNA *in vivo*[91]. This increased flexibility doubtless contributes to dynamic compaction of chromosomal DNA *in vivo*. HU bound in the 34 bp mode should also facilitate formation of DNA loops and bends required for "action at a distance" occurring in Gal repressosome [92] and Mu transpososome [93].

While the physiological significance of the 34 bp mode in DNA compaction and in regulation of other DNA transactions is clear, the occurrence and the significance of the modestly cooperative, relatively unbent 10 bp and 6 bp modes are currently unknown. In exponential growth, the average gap size on the nucleoid is estimated to be at least 160 bp with a ratio [HU]/[160 bp DNA gap] ~ 0.6 (or [DNA bp]/[HU] ~ 270) if the other abundant DNA binding proteins (FIS, H-NS, IHF, RNA polymerase, and CRP) are assumed to be all bound and distributed randomly on the nucleoid [10]. For this condition similar to that for determination of the initial binding heat for 160 bp DNA, the 34 bp mode is predicted to be dominant (i.e., $127k_{34}/(127k_{34}+151k_{10}+155k_6) \sim 0.93$ using values in Table 3; the proportionality of each k_i is the statistical factor of each binding mode), though heterogeneity in gap size would affect this calculation. We expect that gaps smaller than 34 bp can be efficiently filled by the two smaller-site-size, modestly-cooperative modes. The population distribution between the three modes could be shifted by changes in growth conditions or by the presence of other DNA binding proteins [10]. Information about *in vivo* distributions of HU and other NAPs on the nucleoid as a function of growth conditions and growth phase [7] and investigation of possible interactions between the different HU binding modes and other DNA binding proteins [94] will improve our understanding of the physiological significance of each of these modes.

Materials and Methods

Materials

All the chemicals used in these studies were prepared and obtained as described previously [10]. *E.coli* $HU_{\alpha\beta}$ and DNA oligomers

(8 bp DNA: 5′- CTCGCGAG -3′;

15 bp DNA: 5′- CGGTCAGTTCAAGGC –3′;

34 bp DNA: 5′ – GCCAAAAAAGCATTGCTTATCAATTTGTTGCACC –3′;

38 bp DNA: 5′ – CGGTCAGTTCAAGCCCTTCTAAGTTTGTAGACACCAGC –3′;

and 160 bp calf thymus DNA) were also prepared and purified as described previously (8 bp – 38 bp DNA oligomers were initially synthesized and purified by Integrated DNA Technologies (Coraville, IA)) [10]. The purities and binding activities of HU and DNA were essentially the same for independent preparations.

ITC titrations

Samples for ITC experiments were extensively dialyzed (three changes, > 36 hours total) against binding buffer (0.010 M Na_2HPO_4, 0.001 M Na_2EDTA, and NaCl concentration in the range 0.038 M – 0.128 M, pH 7.5) using Spectra/Pore membrane tubing (3500 Da cutoff for HU and 500 Da cutoff for DNA). Forward ITC titrations, where HU was injected into the cell containing DNA, were performed with VP-ITC (MicroCal, LLC, Northhampton, MA). Detailed procedures for centrifuging/degassing the samples, measurements of protein/DNA concentrations, choosing the running parameters of ITC, and determination of dilution/mechanical heats were described previously [10]

For formation of a single type of complex (designated S) from two reactants, the standard ITC equation [95] for the heat $q_{p,i}$ of the *i*th injection, which takes into account the volume displacement in the reaction cell, is:

$$q_{p,i}=\frac{\Delta H_s^{\circ} V_{cell}}{[HU]_{inj} V_{inj}}\{[S]_i - [S]_{i-1}+\frac{V_{inj}}{V_{cell}}(\frac{[S]_i+[S]_{i-1}}{2})\} \quad \text{(Eq. 2)}$$

In Eq. 2, ΔH_s° is the standard enthalpy change for formation of any complex S, V_{cell} is the volume of the reaction cell, $[HU]_{inj}$ is the molar concentration of HU in the injection syringe, V_{inj} is the injection volume, and $[S]_i$ and $[S]_{i-1}$ are the equilibrium molar concentrations of the complex in the cell after *i*th and *i-1*th injection, respectively. To analyze ITC isotherms for binding of HU to DNA oligomers, a sum of heat contributions from the different types of complexes formed (each contribution given by Eq. 2) was used in the nonlinear regression program NONLIN [96] and Igor Pro 5/6. Concentrations $[S]_i$ used in fitting or simulation of binding isotherms and population distributions were obtained by numerically solving the appropriate system of equations involving total concentrations of HU and DNA (mass balance equation) and the partition function for each length of DNA as given in the following sections.

Fittings and simulations of 8 bp and 15 bp DNA binding isotherms

In the salt concentration ($[Na^+]$) range from 0.06 M to 0.125 M, forward titrations of 8 bp DNA with HU were fit to eq. 2 where the general concentration term [S] is the concentration of HU bound in the 6 bp mode ($[HU]_{b,6}$). For each iteration of the fitting procedure, trial values of k_6 and Δh_6 are used to solve the mass balance equation for the total concentration of HU and the partition function for 8 bp DNA ($Z_{8\ bp}$) [10] to obtain the concentration of free HU ($[HU]_{free}$) and $[HU]_{b,6}$:

$$[HU]_{total}=[HU]_{free}+[HU]_{b,6}=[HU]_{free}+[DNA]_{total}\frac{\partial \ln Z_{8\ bp}}{\partial \ln [HU]_{free}} \quad \text{(Eq. 3a)}$$

$$Z_{8\ bp}=1+3k_6[HU]_{free} \quad \text{(Eq. 3b)}$$

The 15 bp DNA binding isotherms of HU were analyzed as a sum of heat contributions ($q_{p,\,i}$ in Eq. 2) from binding of HU to 15 bp DNA in the 10 bp mode ([S] = $[HU]_{b,\,10}$) and the 6 bp mode ([S] = $[HU]_{b,\,6}$) and from formation of a "contact point" between nearest neighbor HU molecules bound in the 6 bp mode ([S] = [contact point]). For each iteration of the fitting procedure (or for final simulation), trial (or best fit) values of k_{10}, Δh_{10}, k_6, Δh_6, ω_6, and $\Delta h_{\omega 6}$ are used to solve the mass balance equation for the total concentration of HU and the partition function for 15 bp DNA ($Z_{15\ bp}$) [10] to obtain $[HU]_{free}$, $[HU]_b$,10, $[HU]_{b,\,6}$, and [contact point]:

$$\begin{aligned}[HU]_{total} &=[HU]_{free}+[HU]_{b,10}+[HU]_{b,6}\\ &=[HU]_{free}+[DNA]_{total}(\frac{\partial \ln Z_{15\ bp}}{\partial \ln k_{10}[HU]_{free}}+\frac{\partial \ln Z_{15\ bp}}{\partial \ln k_6[HU]_{free}})\end{aligned} \quad \text{(Eq. 4a)}$$

$$Z_{15\ bp}=1+(6k_{10}+10k_6)[HU]_{free}+(6+4\omega_6)\,(k_6[HU]_{free})^2 \quad \text{(Eq. 4b)}$$

$$[\text{contact point}]=[\text{DNA}]_{\text{total}}\frac{\partial \ln Z_{15\text{ bp}}}{\partial \ln \omega_6} \quad \text{(Eq. 4c)}$$

Fitting and simulation of 34 bp DNA binding isotherms

The 34 bp DNA binding isotherms of HU were analyzed as a sum of heat contributions ($q_{p,i}$ in Eq. 2) from binding of HU to 34 bp DNA in the 34 bp, the 10 bp, and the 6 bp modes ([S] = $[HU]_{b,34}$, $[HU]_{b,10}$, and $[HU]_{b,6}$) and from formation of three types of contact points between nearest neighbor HU molecules bound in the 10 bp or the 6 bp mode ([S] = $[\text{contact point}]_{10\text{-}10}$, $[\text{contact point}]_{6\text{-}6}$, and $[\text{contact point}]_{10\text{-}6}$). Based on the modified sequence generating function method that we previously developed to describe the competition between the 34 bp, the 10 bp, and the 6 bp modes on 34 bp DNA [10], the mass balance equation for the total concentration of HU is given by:

$$\begin{aligned}[HU]_{\text{total}}&=[HU]_{\text{free}}+[HU]_{b,6}+[HU]_{b,10}+[HU]_{b,34}\\&=[HU]_{\text{free}}+\frac{[DNA]_{\text{total}}x_1^{34}}{x_1^{34}+k_{34}[HU]_{\text{free}}}\left[\frac{\partial \ln x^{34}}{\partial \ln(k_6[HU]_{\text{free}})}+\frac{\partial \ln x^{34}}{\partial \ln(k_{10}[HU]_{\text{free}})}+\frac{k_{34}[HU]_{\text{free}}}{1+k_{34}[HU]_{\text{free}}/x^{34}}\right]_{x=x1}\end{aligned} \quad \text{(Eq. 5)}$$

In Eq. 5, x_1^{34} is the partition function for 34 bp DNA including the free state and bound states in the 10 bp and the 6 bp modes and x_1 is the largest root of the secular equation f(x):

$$\begin{aligned}f(x)=&[HU]_{\text{free}}^2\{k_{10}k_6[(\omega_{10}\omega_6\\&-\omega_{10/6}^2)x\\&+(\omega_{10}+\omega_6-2\omega_{10/6}-\omega_{10}\omega_6+\omega_{10/6}^2)]\}+[HU]_{\text{free}}\{k_6[(\omega_6-1)x^{10}-\omega_6x^{11}]\\&+k_{10}[(\omega_{10}\\&-1)x^6\\&-\omega_{10}x^7]\}\\&+x^{17}-x^{16}=0\end{aligned} \quad \text{(Eq. 6)}$$

For each iteration of the fitting procedure (or for final simulation), trial (or best fit) values of k_{34}, Δh_{34}, k_{10}, Δh_{10}, k_6, Δh_6, ω_{10}, $\Delta h_{\omega 10}$, ω_6, $\Delta h_{\omega 6}$, $\omega_{10/6}$, and $\Delta h_{\omega 10/6}$ are used to simultaneously solve these two equations to obtain x_1, $[HU]_{\text{free}}$, $[HU]_{b,34}$, $[HU]_{b,10}$, and $[HU]_{b,6}$. All three types of [contact point] can be also calculated using the following equations:

$$[\text{contact point}]_i=\frac{[DNA]_{\text{total}}x_1^{34}}{x_1^{34}+k_{34}[HU]_{\text{free}}}\left(\frac{\partial \ln x^{34}}{\partial \ln \omega_i}\right)_{x=x_1} \quad i=10-10,\ 6-6,\ \text{or}\ 10-6 \quad \text{(Eq. 7a)}$$

$$\left(\frac{\partial \ln x}{\partial \ln \omega_i}\right)_{x=x_1}=-\frac{\omega_i}{x_1}\left[\left(\frac{\partial f(x)}{\partial \omega_i}\right)_{x=x_1}/\left(\frac{\partial f(x)}{\partial x}\right)_{x=x_1}\right] \quad \text{(Eq. 7b)}$$

Structural modeling and calculations

The crystal structures of the *Anabaena* HU – TR3 DNA (PDB code 1P71) [21] and the IHF – H′ DNA complexes (PDB code 1IHF) [72] were used as templates to model the structures of the complexes between *E. coli* HU and duplex 34 bp DNA in the 34 bp, the 10 bp, and the 6 bp modes. In modeling the 34 bp mode, the 17 bp DNA in the *Anabaena* HU – TR3 DNA structure was replaced by the 34 bp DNA in the IHF – H′ DNA structure after aligning these two structures using Pymol [97] Then, the overall bend angle of the 34 bp DNA (163°) was reduced to that of the 17 bp DNA (143°) by rotating and aligning the flanking regions of the 34 bp DNA to the corresponding flanking regions of the 17 bp DNA. In modeling the 10 bp mode, the bent 34 bp DNA in the model structure of the 34 bp mode was replaced by a linear duplex 34 bp DNA (obtained from the *make-na* web server and the *nucleic acid builder* program developed by Case and co-workers: http://structure.usc.edu/make-na/) after aligning the central 10 bp regions of these two DNA molecules. Then, the flexible arm regions of HU (residues 57 – 73) were moved out of the DNA minor grooves to obtain a binding site size of approximately 10 bp and to minimize steric clash of these regions with DNA phosphate backbone/bases. Subsequently, this structure was used to model the 6 bp mode by rotating the HU molecule around the axis perpendicular to the DNA helical axis by 50° to reduce the binding site size from 10 bp to 6 bp.

A homology model of *E. coli* $HU_{\alpha\beta}$ was calculated using Swiss Model (http://swissmodel.expasy.org/) [98; 99]. Models of EHU_{α} and EHU_{β} were calculated using the A and B chains from 1P71 [21] as templates, respectively. These models were then assembled to form the *E. coli* $HU_{\alpha\beta}$ dimer by superposing the alpha carbon backbone residues 2–88 on those in the dimer from 1P71 using InsightII. The 34 bp mode complex was then modeled by superposing the *E. coli* $HU_{\alpha\beta}$ model dimer on the structure modeled above with a DNA bend angle of 143°. For the 10 bp and the 6 bp modes, the core residues (2–50) were superposed on the respective DNA models above. Because the arms are modeled out of the minor groves, the arms (57–73) were superposed independently. These independent superpositions were then assembled into a HU dimer bound in either the 10 bp or 6 bp mode using InsightII. Steric clash was removed using the side chain rotamer library in InsightII.

Using these models, the number of cationic and anionic residues of HU within 3 Å -10 Å from DNA phosphate oxygens were calculated using Pymol [97] Water (solvent) accessible surface areas (ASA) of the model structures were calculated for both HU – DNA complexes and unbound HU and DNA (obtained by removing DNA or HU coordinates in the PDB codes) using Surface Racer [100] with a probe radius of 1.4 Å and accepted values of the van der Waals radii [101].

These homology models were compared to the crystal structures of the $HU_{\alpha\beta}$heterodimer (2O97)[102] and the HU_{α}subunit (1MUL)[59] from *E.coli* without DNA and DNA binding arms. Superposition of the homology model (34 bp mode) on the heterodimer (2O97) and on the HU_{α} subunit (1MUL) yields rms deviations of 0.58 Å and 0.52 Å, respectively, indicating equivalent overall folding for these three structures. Side chain conformations of charged amino acid residues of these two published structures were also examined to identify any charged residue interacting with DNA phosphates but not detected in our homology model. For 2O97, αK51, αK83, αK86, βK53, βR55, βR58, and βK86 are within 8 Å of DNA phosphates and all these residues are also detected in the homology model. βR80 and βK83 are detected only in the homology model. For 1 MUL, only αK86 is within 8 Å of a DNA phosphate, and αK51 and αR55 are resolved only to the C delta atoms of the side chains. In summary, the homology model built in this study captures the correct overall folding and all possible charge-charge interaction pairs for the HU-DNA complex.

Numerical NLPB calculations of Coulombic free energy changes for formations of model structures for the three HU-DNA binding modes as a function of salt concentration

The change in Coulombic standard free energy (ΔG^{Coul}) for formation of a small site size mode (10 bp or 6 bp) complex of HU on 34 bp DNA is estimated from the Coulombic free energy change for rigid-body docking (ΔG^{Coul}_{dock}), assuming that conformational changes in HU coupled to binding are not significant.

$$\Delta G^{Coul}=\Delta G^{Coul}_{dock}=G^{Coul}_{C}-G^{Coul}_{P}-G^{Coul}_{D} \quad \text{(Eq. 8)}$$

where G^{Coul}_{C}, G^{Coul}_{D}, and G^{Coul}_{P} are Coulombic standard free energies of the model complex (C), of free DNA (D: obtained by removing HU coordinates from C), and of free protein (P: obtained by removing DNA coordinates from C). For the 34 bp binding mode, ΔG^{Coul} is calculated using G^{Coul}_{C} and G^{Coul}_{P} from the model for the 34 bp mode complex, and G^{Coul}_{D} from the linear 34 bp DNA structure used in models of the 10 bp and 6 bp mode complexes, in order to include the Coulombic free energy change for DNA bending. (No other DNA conformational changes are invoked.)

The Coulombic free energies are calculated by Adaptive Poisson-Boltzmann Solver (APBS) [79] with the Amber force field. PDB files were converted to format required for APBS input with online converter [103]. APBS solves the nonlinear Poisson-Boltzmann (NLPB) equation numerically for an all-atom molecular model of a biopolymer and calculates its standard free energy (standard chemical potential), which differs from G^{Coul} (Eq. 8) by a salt concentration independent contribution that we determine from the high salt limit of the NLPB-calculated free energy [104]. Structural models of the three binding modes (Fig. 9) were used for these calculations. Cell sizes and grid point spacings were chosen as described previously in detail [104] and an initial focusing procedure was applied, in order to obtain accurate and efficient calculations. Small ion radii were set at 2 Å; the external dielectric constant was set at 78.5 (water, 25 °C) and a value of 2 was chosen for the internal dielectric constant. NLPB values of G^{Coul}_{C}, G^{Coul}_{D}, and G^{Coul}_{P} calculated at univalent salt concentrations of 0.06 M, 0.082 M, 0.1 M, 0.125 M, 0.15 M, 0.175 M and 0.2 M were used to calculate ΔG^{Coul}. The Coulombic contribution to the salt concentration dependence of the binding free energy ($SK^{Coul}=-\frac{\partial \Delta G^{Coul}/RT}{\partial \ln[M^{+}]}$) is then determined from the slope of the plot of ΔG^{Coul} vs. $\ln[M^{+}]$.

In order to obtain average values of SK^{Coul} for the ensemble of all potential binding sites on 34 bp DNA for the 10 bp mode (25 sites) and the 6 bp mode (29 sites), the DNA in each structural model (Fig. 9) was shifted along its helical axis by j base pairs (j = ±1, ±2…). Values of ΔG^{Coul} and SK^{Coul} were calculated as outlined above for each position (j) of the complex. Then, an ensemble-average SK^{Coul} was obtained from a sum of SK^{Coul} for all positions weighted by $\exp(-\Delta G^{Coul}_{j}/\mathrm{RT})/\sum_{j}\exp(-\Delta G^{Coul}_{j}/\mathrm{RT})$. Parallel calculations were performed for all positions of the 10 bp and the 6 bp mode complexes on 15 bp DNA, and of the 6 bp mode complex on 8 bp DNA.

Prediction of Coulombic end effects (CEE) on the binding constants of the 10 bp (k_{10}) and the 6 bp (k_6) modes as a function of DNA length using the analytical CEE model

The fold-increases in k_{10} and k_6 from 8 bp to 15 bp DNA and from 15 bp to 34 bp DNA (i.e., $k_{6,\ 15bp}/k_{6,\ 8bp}$, $k_{6,\ 34bp}/k_{6,\ 15bp}$, and $k_{10,\ 34bp}/k_{10,\ 15bp}$) caused by CEEs were estimated

using the so-called CEE model [56] for binding of an oligocation ligand to a DNA oligomer. The model predicts the binding free energy $\Delta g_{ij}°$ and corresponding log-log salt concentration derivative Sk_{ij} for a complex involving binding mode i where the ligand position is described by index *j*, the number of phosphate charges in the unoccupied region between the nearer end and the bound region. Then, the position-averaged binding constant for a given mode and DNA length is the average of $e^{-\Delta gi,j\circ/RT}$ over all potential binding sites (*j*) on DNA. The position-averaged Sk_i is a sum of $Sk_{i,j}$ weighted by $e^{-\Delta gi,j\circ/RT} / \Sigma_j e^{-\Delta gi,j\circ/RT}$ In applying the oligocation binding model, DNA length is expressed as the number of phosphate charges (Z_D: for N bp DNA like those oligomers studied here, without terminal phosphates, $Z_D = 2N - 2$). Other input quantities for the oligocation model include the effective net charge on the DNA binding interface of HU (Z_L), the length of the "end" region of DNA expressed as a number of phosphate charges (N_e), and the coefficients describing a CEE for the chemical potential (G_1) and salt ion association (J_1) of a short DNA oligomer. Detailed discussions of these quantities are provided in Shkel *et al.* (2006). Values of Z_D are 14, 28, and 66 for 8 bp, 15 bp, and 34 bp DNA oligomers, respectively. Values of Z_L are +8 and +9 for the 10 bp and the 6 bp modes, respectively, based on the values of polymeric Sk_i ($= Sk_{i,\infty} = -0.89Z_L$) which are estimated from the all-atom NLPB calculations of Sk_i for these modes on 34 bp DNA (-8.2 and -7.3 for the 10 bp and the 6 bp modes, respectively). Values of N_e, G_1, and J_1 are 12 phosphates at each end, 0.015 kcal/mol (for 0.15 M Na^+), and 0.019, respectively [56].

The position index *j* was assigned to potential binding sites for a given mode, starting from the most central complex with *j*=Q/2 where Q is the number of phosphate charges unoccupied after binding of HU. Then, *j* changes by ± 2 as HU moves along DNA with a step of one base pair to each end of DNA until the total number of the complexes considered reaches $N - n_i + 1$.

From comparison of Sk_{ij} from the quadratic model to all-atom NLPB results, we found that $Q = Z_D - Z_L$ for the 10 bp mode and $Q = Z_D - Z_L + 5$ for the 6 bp mode. At 0.15 Na^+, $\Delta g_{i,j}°$ and $Sk_{i,j}$ are given by eqs. 28, 29, 20, and 21 of Shkel *et al.* (2006) for the 6 bp mode on 8 bp DNA, by eqs. 30, 31, 22, and 23 for the 6 bp mode on 15 bp and 34 bp DNA and the 10 bp mode on 34 bp DNA, and by eqs. 28, 29, 22, and 23 for the 10 bp mode on 15 bp DNA. Therefore, the fold-increases in the binding constants for the 10 bp and the 6 bp modes between different DNA lengths can be calculated at 0.15 M Na^+, and the difference in Sk_i between different DNA lengths allows calculations of the fold-increases in the binding constants at other salt concentrations.

Supplementary Material

Refer to Web version on PubMed Central for supplementary material.

Acknowledgments

We thank Reid Johnson (UCLA) for providing the *E. coli* strain for over-expressing HU and its purification protocol, Wlodek Bujalowski (UTMB) for helping initial computational set up in SGF analysis, Kirk Vander Muelen (UW-Madison) for providing the residue distance calculation program and helpful discussions, Mike Capp (UW-Madison) for assistance in HU over-expression and preparation of 160 bp calf thymus DNA, and Darrel McCaslin (UW-Madison, Biophysics Instrumentation Facility) for technical advice. This work was supported by NIH grant GM23467.

References

1. Johnson, RC.; Johnson, LM.; Schmidt, JW.; Gardner, JF. Major Nucleoid Proteins in the Structure and Function of the *Escherichia coli* Chromosome. In: Higgins, NP., editor. The Bacterial Chromosome. ASM Press; Washington, D.C: 2005. p. 65-132.

2. Drlica K, Rouviere-Yaniv J. Histonelike proteins of bacteria. Microbiol Rev. 1987; 51:301–19. [PubMed: 3118156]
3. Arfin SM, Long AD, Ito ET, Tolleri L, Riehle MM, Paegle ES, Hatfield GW. Global gene expression profiling in Escherichia coli K12. The effects of integration host factor. J Biol Chem. 2000; 275:29672–84. [PubMed: 10871608]
4. Friedman DI. Integration host factor: a protein for all reasons. Cell. 1988; 55:545–54. [PubMed: 2972385]
5. Stavans J, Oppenheim A. DNA-protein interactions and bacterial chromosome architecture. Phys Biol. 2006; 3:R1–10. [PubMed: 17200598]
6. Swinger KK, Rice PA. IHF and HU: flexible architects of bent DNA. Curr Opin Struct Biol. 2004; 14:28–35. [PubMed: 15102446]
7. Azam TA, Ishihama A. Twelve species of the nucleoid-associated protein from Escherichia coli. Sequence recognition specificity and DNA binding affinity. J Biol Chem. 1999; 274:33105–13. [PubMed: 10551881]
8. Luijsterburg MS, Noom MC, Wuite GJ, Dame RT. The architectural role of nucleoid-associated proteins in the organization of bacterial chromatin: a molecular perspective. J Struct Biol. 2006; 156:262–72. [PubMed: 16879983]
9. Luger K, Mader AW, Richmond RK, Sargent DF, Richmond TJ. Crystal structure of the nucleosome core particle at 2.8 A resolution. Nature. 1997; 389:251–60. [PubMed: 9305837]
10. Koh J, Saecker RM, Record MT Jr. DNA Binding Mode Transitions of Escherichia coli HU(alphabeta): Evidence for Formation of a Bent DNA - Protein Complex on Intact, Linear Duplex DNA. J Mol Biol. 2008; 383:324–346. [PubMed: 18657548]
11. van Noort J, Verbrugge S, Goosen N, Dekker C, Dame RT. Dual architectural roles of HU: Formation of flexible hinges and rigid filaments. Proceedings of the National Academy of Sciences of the United States of America. 2004; 101:6969–6974. [PubMed: 15118104]
12. Skoko D, Wong B, Johnson RC, Marko JF. Micromechanical analysis of the binding of DNA-bending proteins HMGB1, NHP6A, and HU reveals their ability to form highly stable DNA-protein complexes. Biochemistry. 2004; 43:13867–13874. [PubMed: 15504049]
13. Dame RT, Goosen N. HU: promoting or counteracting DNA compaction? FEBS Lett. 2002; 529:151–6. [PubMed: 12372591]
14. Bonnefoy E, Rouviere-Yaniv J. HU and IHF, two homologous histone-like proteins of Escherichia coli, form different protein-DNA complexes with short DNA fragments. EMBO J. 1991; 10:687–96. [PubMed: 2001682]
15. Pinson V, Takahashi M, Rouviere-Yaniv J. Differential binding of the Escherichia coli HU, homodimeric forms and heterodimeric form to linear, gapped and cruciform DNA. J Mol Biol. 1999; 287:485–97. [PubMed: 10092454]
16. Wojtuszewski K, Hawkins ME, Cole JL, Mukerji I. HU binding to DNA: Evidence for multiple complex formation and DNA bending (vol 40, pg 2588, 2001). Biochemistry. 2001; 40:4892–4892.
17. Wojtuszewski K, Mukerji I. HU binding to bent DNA: A fluorescence resonance energy transfer and anisotropy study. Biochemistry. 2003; 42:3096–3104. [PubMed: 12627977]
18. Benevides JM, Danahy J, Kawakami J, Thomas GJ Jr. Mechanisms of specific and nonspecific binding of architectural proteins in prokaryotic gene regulation. Biochemistry. 2008; 47:3855–62. [PubMed: 18302340]
19. Rouviere-Yaniv J, Yaniv M, Germond JE. E. coli DNA binding protein HU forms nucleosomelike structure with circular double-stranded DNA. Cell. 1979; 17:265–74. [PubMed: 222478]
20. Broyles SS, Pettijohn DE. Interaction of the Escherichia coli HU protein with DNA. Evidence for formation of nucleosome-like structures with altered DNA helical pitch. J Mol Biol. 1986; 187:47–60. [PubMed: 3514923]
21. Swinger KK, Lemberg KM, Zhang Y, Rice PA. Flexible DNA bending in HU-DNA cocrystal structures. Embo J. 2003; 22:3749–60. [PubMed: 12853489]
22. Tanaka I, Appelt K, Dijk J, White SW, Wilson KS. 3-A resolution structure of a protein with histone-like properties in prokaryotes. Nature. 1984; 310:376–81. [PubMed: 6540370]

23. Lohman TM, Overman LB. Two binding modes in Escherichia coli single strand binding protein-single stranded DNA complexes. Modulation by NaCl concentration. J Biol Chem. 1985; 260:3594–603. [PubMed: 3882711]
24. Bujalowski W, Lohman TM. Escherichia coli single-strand binding protein forms multiple, distinct complexes with single-stranded DNA. Biochemistry. 1986; 25:7799–802. [PubMed: 3542037]
25. Bujalowski W, Overman LB, Lohman TM. Binding mode transitions of Escherichia coli single strand binding protein-single-stranded DNA complexes. Cation, anion, pH, and binding density effects. J Biol Chem. 1988; 263:4629–40. [PubMed: 3280566]
26. Lohman TM, Ferrari ME. Escherichia coli single-stranded DNA-binding protein: multiple DNA-binding modes and cooperativities. Annu Rev Biochem. 1994; 63:527–70. [PubMed: 7979247]
27. Kumaran S, Kozlov AG, Lohman TM. Saccharomyces cerevisiae replication protein A binds to single-stranded DNA in multiple salt-dependent modes. Biochemistry. 2006; 45:11958–73. [PubMed: 17002295]
28. Rajendran S, Jezewska MJ, Bujalowski W. Human DNA polymerase beta recognizes single-stranded DNA using two different binding modes. J Biol Chem. 1998; 273:31021–31. [PubMed: 9813000]
29. Jezewska MJ, Rajendran S, Bujalowski W. Transition between different binding modes in rat DNA polymerase beta-ssDNA complexes. J Mol Biol. 1998; 284:1113–31. [PubMed: 9837730]
30. Record MT Jr, Zhang W, Anderson CF. Analysis of effects of salts and uncharged solutes on protein and nucleic acid equilibria and processes: a practical guide to recognizing and interpreting polyelectrolyte effects, Hofmeister effects, and osmotic effects of salts. Adv Protein Chem. 1998; 51:281–353. [PubMed: 9615173]
31. Record MT Jr, Anderson CF, Lohman TM. Thermodynamic analysis of ion effects on the binding and conformational equilibria of proteins and nucleic acids: the roles of ion association or release, screening, and ion effects on water activity. Q Rev Biophys. 1978; 11:103–78. [PubMed: 353875]
32. Vander Meulen KA, Saecker RM, Record MT Jr. Formation of a wrapped DNA-protein interface: experimental characterization and analysis of the large contributions of ions and water to the thermodynamics of binding IHF to H′ DNA. J Mol Biol. 2008; 377:9–27. [PubMed: 18237740]
33. Pegram LM, Record MT Jr. Thermodynamic origin of hofmeister ion effects. J Phys Chem B. 2008; 112:9428–36. [PubMed: 18630860]
34. Record MT Jr, Lohman ML, De Haseth P. Ion effects on ligand-nucleic acid interactions. J Mol Biol. 1976; 107:145–58. [PubMed: 1003464]
35. Mascotti DP, Lohman TM. Thermodynamic extent of counterion release upon binding oligolysines to single-stranded nucleic acids. Proc Natl Acad Sci U S A. 1990; 87:3142–6. [PubMed: 2326273]
36. Olmsted MC, Bond JP, Anderson CF, Record MT Jr. Grand canonical Monte Carlo molecular and thermodynamic predictions of ion effects on binding of an oligocation (L8+) to the center of DNA oligomers. Biophys J. 1995; 68:634–47. [PubMed: 7696515]
37. Misra VK, Honig B. On the magnitude of the electrostatic contribution to ligand-DNA interactions. Proc Natl Acad Sci U S A. 1995; 92:4691–5. [PubMed: 7753866]
38. Sharp KA, Friedman RA, Misra V, Hecht J, Honig B. Salt effects on polyelectrolyte-ligand binding: comparison of Poisson-Boltzmann, and limiting law/counterion binding models. Biopolymers. 1995; 36:245–62. [PubMed: 7492748]
39. Lohman TM, deHaseth PL, Record MT Jr. Pentalysine-deoxyribonucleic acid interactions: a model for the general effects of ion concentrations on the interactions of proteins with nucleic acids. Biochemistry. 1980; 19:3522–30. [PubMed: 7407056]
40. Braunlin WH, Strick TJ, Record MT Jr. Equilibrium dialysis studies of polyamine binding to DNA. Biopolymers. 1982; 21:1301–14. [PubMed: 7115891]
41. Mascotti DP, Lohman TM. Thermodynamics of single-stranded RNA binding to oligolysines containing tryptophan. Biochemistry. 1992; 31:8932–46. [PubMed: 1382582]
42. Mascotti DP, Lohman TM. Thermodynamics of single-stranded RNA and DNA interactions with oligolysines containing tryptophan. Effects of base composition. Biochemistry. 1993; 32:10568–79. [PubMed: 7691177]
43. Mascotti DP, Lohman TM. Thermodynamics of oligoarginines binding to RNA and DNA. Biochemistry. 1997; 36:7272–9. [PubMed: 9188729]

44. Frank DE, Saecker RM, Bond JP, Capp MW, Tsodikov OV, Melcher SE, Levandoski MM, Record MT Jr. Thermodynamics of the interactions of lac repressor with variants of the symmetric lac operator: effects of converting a consensus site to a non-specific site. J Mol Biol. 1997; 267:1186–206. [PubMed: 9150406]
45. McAfee JG, Edmondson SP, Zegar I, Shriver JW. Equilibrium DNA binding of Sac7d protein from the hyperthermophile Sulfolobus acidocaldarius: fluorescence and circular dichroism studies. Biochemistry. 1996; 35:4034–45. [PubMed: 8672437]
46. Robinson H, Gao YG, McCrary BS, Edmondson SP, Shriver JW, Wang AH. The hyperthermophile chromosomal protein Sac7d sharply kinks DNA. Nature. 1998; 392:202–5. [PubMed: 9515968]
47. Lundback T, Hard T. Salt dependence of the free energy, enthalpy, and entropy of nonsequence specific DNA binding. J Phys Chem. 1996; 100:17690–17695.
48. Gao YG, Su SY, Robinson H, Padmanabhan S, Lim L, McCrary BS, Edmondson SP, Shriver JW, Wang AH. The crystal structure of the hyperthermophile chromosomal protein Sso7d bound to DNA. Nat Struct Biol. 1998; 5:782–6. [PubMed: 9731772]
49. Dragan AI, Liggins JR, Crane-Robinson C, Privalov PL. The energetics of specific binding of AT-hooks from HMGA1 to target DNA. J Mol Biol. 2003; 327:393–411. [PubMed: 12628246]
50. Dragan AI, Klass J, Read C, Churchill ME, Crane-Robinson C, Privalov PL. DNA binding of a non-sequence-specific HMG-D protein is entropy driven with a substantial non-electrostatic contribution. J Mol Biol. 2003; 331:795–813. [PubMed: 12909011]
51. Dragan AI, Read CM, Makeyeva EN, Milgotina EI, Churchill ME, Crane-Robinson C, Privalov PL. DNA binding and bending by HMG boxes: energetic determinants of specificity. J Mol Biol. 2004; 343:371–93. [PubMed: 15451667]
52. Olmsted MC, Anderson CF, Record MT Jr. Importance of oligoelectrolyte end effects for the thermodynamics of conformational transitions of nucleic acid oligomers: a grand canonical Monte Carlo analysis. Biopolymers. 1991; 31:1593–604. [PubMed: 1814506]
53. Zhang W, Bond JP, Anderson CF, Lohman TM, Record MT Jr. Large electrostatic differences in the binding thermodynamics of a cationic peptide to oligomeric and polymeric DNA. Proc Natl Acad Sci U S A. 1996; 93:2511–6. [PubMed: 8637905]
54. Zhang W, Ni H, Capp MW, Anderson CF, Lohman TM, Record MT Jr. The importance of coulombic end effects: experimental characterization of the effects of oligonucleotide flanking charges on the strength and salt dependence of oligocation (L8+) binding to single-stranded DNA oligomers. Biophys J. 1999; 76:1008–17. [PubMed: 9916032]
55. Ballin JD, Shkel IA, Record MT Jr. Interactions of the KWK6 cationic peptide with short nucleic acid oligomers: demonstration of large Coulombic end effects on binding at 0.1-0.2 M salt. Nucleic Acids Res. 2004; 32:3271–81. [PubMed: 15205469]
56. Shkel IA, Ballin JD, Record MT Jr. Interactions of cationic ligands and proteins with small nucleic acids: analytic treatment of the large coulombic end effect on binding free energy as a function of salt concentration. Biochemistry. 2006; 45:8411–26. [PubMed: 16819840]
57. Olmsted MC, Anderson CF, Record MT Jr. Monte Carlo description of oligoelectrolyte properties of DNA oligomers: range of the end effect and the approach of molecular and thermodynamic properties to the polyelectrolyte limits. Proc Natl Acad Sci U S A. 1989; 86:7766–70. [PubMed: 2813356]
58. Stein VM, Bond JP, Capp MW, Anderson CF, Record MT Jr. Importance of coulombic end effects on cation accumulation near oligoelectrolyte B-DNA: a demonstration using 23Na NMR. Biophys J. 1995; 68:1063–72. [PubMed: 7756526]
59. Ramstein J, Hervouet N, Coste F, Zelwer C, Oberto J, Castaing B. Evidence of a thermal unfolding dimeric intermediate for the Escherichia coli histone-like HU proteins: thermodynamics and structure. J Mol Biol. 2003; 331:101–21. [PubMed: 12875839]
60. Koh, J. Ph D thesis. University of Wisconsin-Madison; 2008. Thermodynamics of interactions of Escherichia coli HU(alpha, beta) with duplex DNA.
61. McGhee JD, von Hippel PH. Theoretical aspects of DNA-protein interactions: co-operative and non-co-operative binding of large ligands to a one-dimensional homogeneous lattice. J Mol Biol. 1974; 86:469–89. [PubMed: 4416620]

62. Epstein IR. Cooperative and non-cooperative binding of large ligands to a finite one-dimensional lattice. A model for ligand-oligonucleotide interactions. Biophys Chem. 1978; 8:327–39. [PubMed: 728537]
63. Xiao B, Johnson RC, Marko JF. Modulation of HU-DNA interactions by salt concentration and applied force. Nucleic Acids Res. 38:6176–85. [PubMed: 20497998]
64. Ferrari ME, Bujalowski W, Lohman TM. Co-operative binding of Escherichia coli SSB tetramers to single-stranded DNA in the (SSB)35 binding mode. J Mol Biol. 1994; 236:106–23. [PubMed: 8107097]
65. Bujalowski W, Lohman TM. Negative co-operativity in Escherichia coli single strand binding protein-oligonucleotide interactions. I. Evidence and a quantitative model. J Mol Biol. 1989; 207:249–68. [PubMed: 2661832]
66. Bujalowski W, Lohman TM. Negative co-operativity in Escherichia coli single strand binding protein-oligonucleotide interactions. II. Salt, temperature and oligonucleotide length effects. J Mol Biol. 1989; 207:269–88. [PubMed: 2661833]
67. Polach KJ, Widom J. Mechanism of protein access to specific DNA sequences in chromatin: a dynamic equilibrium model for gene regulation. J Mol Biol. 1995; 254:130–49. [PubMed: 7490738]
68. Li G, Widom J. Nucleosomes facilitate their own invasion. Nat Struct Mol Biol. 2004; 11:763–9. [PubMed: 15258568]
69. Poirier MG, Oh E, Tims HS, Widom J. Dynamics and function of compact nucleosome arrays. Nat Struct Mol Biol. 2009; 16:938–44. [PubMed: 19701201]
70. Courtenay ES, Capp MW, Saecker RM, Record MT Jr. Thermodynamic analysis of interactions between denaturants and protein surface exposed on unfolding: interpretation of urea and guanidinium chloride m-values and their correlation with changes in accessible surface area (ASA) using preferential interaction coefficients and the local-bulk domain model. Proteins. 2000 4:72–85. [PubMed: 11013402]
71. Courtenay ES, Capp MW, Record MT Jr. Thermodynamics of interactions of urea and guanidinium salts with protein surface: relationship between solute effects on protein processes and changes in water-accessible surface area. Protein Sci. 2001; 10:2485–97. [PubMed: 11714916]
72. Rice PA, Yang SW, Mizuuchi K, NAsh HA. Crystal structure of an IHF-DNA complex: A protein-induced DNA u-turn. Cell. 1996; 87:1295–1306. [PubMed: 8980235]
73. Vivas P, Kuznetsov SV, Ansari A. New insights into the transition pathway from nonspecific to specific complex of DNA with Escherichia coli integration host factor. J Phys Chem B. 2008; 112:5997–6007. [PubMed: 18461910]
74. Vis H, Mariani M, Vorgias CE, Wilson KS, Kaptein R, Boelens R. Solution structure of the HU protein from Bacillus stearothermophilus. J Mol Biol. 1995; 254:692–703. [PubMed: 7500343]
75. Boelens R, Vis H, Vorgias CE, Wilson KS, Kaptein R. Structure and dynamics of the DNA binding protein HU from Bacillus stearothermophilus by NMR spectroscopy. Biopolymers. 1996; 40:553–9. [PubMed: 9101760]
76. White SW, Appelt K, Wilson KS, Tanaka I. A protein structural motif that bends DNA. Proteins. 1989; 5:281–8. [PubMed: 2508086]
77. White SW, Wilson KS, Appelt K, Tanaka I. The high-resolution structure of DNA-binding protein HU from Bacillus stearothermophilus. Acta Crystallogr D Biol Crystallogr. 1999; 55:801–9. [PubMed: 10089311]
78. Christodoulou E, Rypniewski WR, Vorgias CR. High-resolution X-ray structure of the DNA-binding protein HU from the hyper-thermophilic Thermotoga maritima and the determinants of its thermostability. Extremophiles. 2003; 7:111–22. [PubMed: 12664263]
79. Baker NA, Sept D, Joseph S, Holst MJ, McCammon JA. Electrostatics of nanosystems: application to microtubules and the ribosome. Proc Natl Acad Sci U S A. 2001; 98:10037–41. [PubMed: 11517324]
80. Lammi M, Paci M, Gualerzi CO. Proteins from the prokaryotic nucleoid. The interaciton between protein NS and DNA involves the oligomeric form of the protein and at least one Arg residue. FEBS Lett. 1984; 170:99–104.

81. Shindo H, Kurumizaka H, Furubayashi A, Sakuma C, Matsumoto U, Yanagida A, Goshima N, Kano Y, Imamoto F. Proton NMR study on a histone-like protein, HU alpha, from Escherichia coli and its complex with oligo DNAs. Biol Pharm Bull. 1993; 16:437–43. [PubMed: 8364487]
82. Saitoh F, Kawamura S, Yamasaki N, Tanaka I, Kimura M. Arginine-55 in the beta-arm is essential for the activity of DNA-binding protein HU from Bacillus stearothermophilus. Biosci Biotechnol Biochem. 1999; 63:2232–5. [PubMed: 10664859]
83. Goshima N, Kohno K, Imamoto F, Kano Y. HU-1 mutants of Escherichia coli deficient in DNA binding. Gene. 1990; 96:141–5. [PubMed: 2265752]
84. Kozlov AG, Lohman TM. Calorimetric studies of E-coli SSB protein single-stranded DNA interactions. Effects of monovalent salts on binding enthalpy. Journal of Molecular Biology. 1998; 278:999–1014. [PubMed: 9600857]
85. Kozlov AG, Lohman TM. Effects of monovalent anions on a temperature-dependent heat capacity change for Escherichia coli SSB tetramer binding to single-stranded DNA. Biochemistry. 2006; 45:5190–205. [PubMed: 16618108]
86. Lohman TM, Overman LB, Ferrari ME, Kozlov AG. A highly salt-dependent enthalpy change for Escherichia coli SSB protein-nucleic acid binding due to ion-protein interactions. Biochemistry. 1996; 35:5272–9. [PubMed: 8611514]
87. Holbrook JA, Tsodikov OV, Saecker RM, Record MT Jr. Specific and non-specific interactions of integration host factor with DNA: thermodynamic evidence for disruption of multiple IHF surface salt-bridges coupled to DNA binding. J Mol Biol. 2001; 310:379–401. [PubMed: 11428896]
88. Jen-Jacobson L, Engler LE, Jacobson LA. Structural and thermodynamic strategies for site-specific DNA binding proteins. Structure. 2000; 8:1015–23. [PubMed: 11080623]
89. Holbrook JA, Capp MW, Saecker RM, Record MT Jr. Enthalpy and heat capacity changes for formation of an oligomeric DNA duplex: interpretation in terms of coupled processes of formation and association of single-stranded helices. Biochemistry. 1999; 38:8409–22. [PubMed: 10387087]
90. Privalov PL, Dragan AI, Crane-Robinson C, Breslauer KJ, Remeta DP, Minetti CA. What drives proteins into the major or minor grooves of DNA? J Mol Biol. 2007; 365:1–9. [PubMed: 17055530]
91. Law SM, Bellomy GR, Schlax PJ, Record MT Jr. In vivo thermodynamic analysis of repression with and without looping in lac constructs. Estimates of free and local lac repressor concentrations and of physical properties of a region of supercoiled plasmid DNA in vivo. J Mol Biol. 1993; 230:161–73. [PubMed: 8450533]
92. Aki T, Adhya S. Repressor induced site-specific binding of HU for transcriptional regulation. Embo J. 1997; 16:3666–74. [PubMed: 9218807]
93. Lavoie BD, Shaw GS, Millner A, Chaconas G. Anatomy of a flexer-DNA complex inside a higher-order transposition intermediate. Cell. 1996; 85:761–71. [PubMed: 8646783]
94. Flashner Y, Gralla JD. DNA dynamic flexibility and protein recognition: differential stimulation by bacterial histone-like protein HU. Cell. 1988; 54:713–21. [PubMed: 3044609]
95. Microcal, I. ITC Data Analysis in Origin. 2004. p. 104-106.
96. Johnson ML, Frasier SG. Nonlinear least-squares analysis. Methods Enzymol. 1985; 117:301–342.
97. Delano, WK. The PyMol Molecular Graphics System. 2002.
98. Arnold K, Bordoli L, Kopp J, Schwede T. The SWISS-MODEL workspace: a web-based environment for protein structure homology modelling. Bioinformatics. 2006; 22:195–201. [PubMed: 16301204]
99. Kiefer F, Arnold K, Kunzli M, Bordoli L, Schwede T. The SWISS-MODEL Repository and associated resources. Nucleic Acids Res. 2009; 37:D387–92. [PubMed: 18931379]
100. Tsodikov OV, Record MT Jr, Sergeev YV. Novel computer program for fast exact calculation of accessible and molecular surface areas and average surface curvature. J Comput Chem. 2002; 23:600–9. [PubMed: 11939594]
101. Livingstone JR, Spolar RS, Record MT Jr. Contribution to the thermodynamics of protein folding from the reduction in water-accessible nonpolar surface area. Biochemistry. 1991; 30:4237–44. [PubMed: 2021617]
102. Guo F, Adhya S. Spiral structure of Escherichia coli HUalphabeta provides foundation for DNA supercoiling. Proc Natl Acad Sci U S A. 2007; 104:4309–14. [PubMed: 17360520]

103. Dolinsky TJ, Czodrowski P, Li H, Nielsen JE, Jensen JH, Klebe G, Baker NA. PDB2PQR: expanding and upgrading automated preparation of biomolecular structures for molecular simulations. Nucleic Acids Res. 2007; 35:W522–5. [PubMed: 17488841]

104. Shkel IA. Coulombic free energy of polymeric nucleic acid: low- and high-salt analytical approximations for the cylindrical Poisson-Boltzmann model. J Phys Chem B. 2010; 114:10793–803. [PubMed: 20681741]

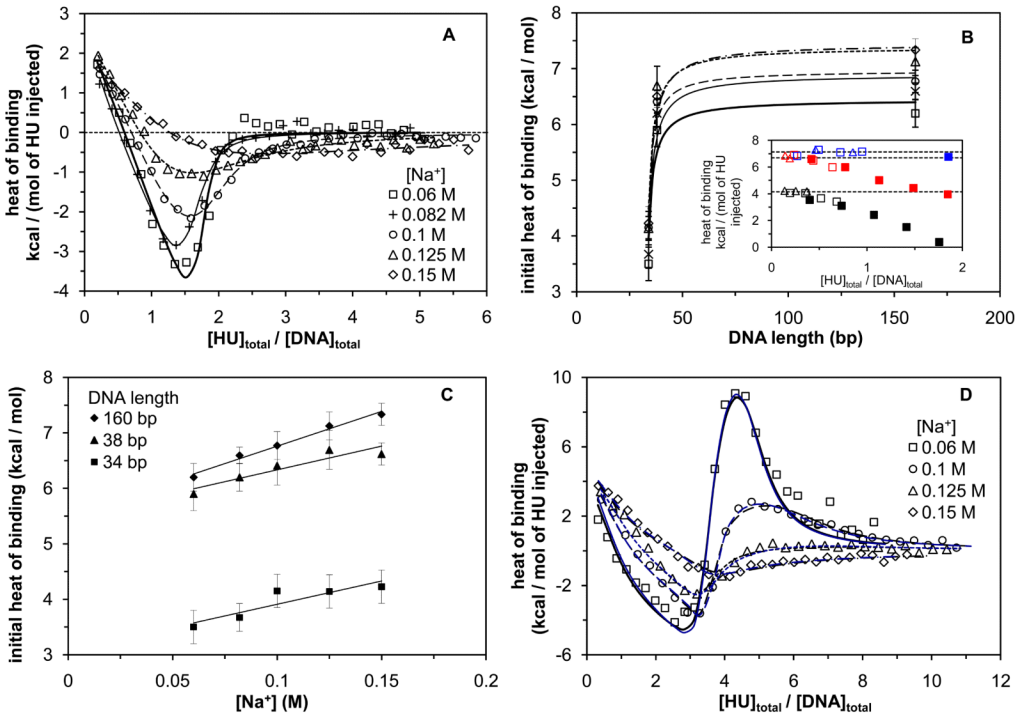

Figure 1.

[HU]/[DNA] and DNA length dependent DNA binding mode transitions of HU detected by ITC in the salt concentration range 0.06 M – 0.15 M Na^+ at 15 °C. Data for 0.15 M Na^+ were reproduced from Koh *et al* (2008). (A) Representative titrations of 15 bp DNA with HU monitored by ITC at 0.06 M (square), 0.082 M (cross), 0.1 M (circle), 0.125 M (triangle), and 0.15 M (diamond) Na^+. Typical concentrations of HU in ITC injection syringe and of DNA in the reaction cell were 100 μM and 4 μM, respectively. Titration data were fit to Eq. 2 and 4 to obtain thermodynamic parameters listed in Table 2. Curves are simulated binding isotherms with the best fit parameters for $k_{6,\ 15bp}/k_{6,\ 8bp} = 1$. (B) DNA length (34 bp – 160 bp) dependence of the initial heat of binding at 0.06 M (square), 0.082 M (x), 0.1 M (circle), 0.125 M (triangle), and 0.15 M (diamond) Na^+. Inset shows the representative titrations using high concentrations of DNA for determination of the initial heat of binding for 34 bp (black), 38 bp (red), and 160 bp (blue) DNA at 0.125 M Na^+. The observed DNA length dependence at each salt concentration was analyzed using Eq. 1 to obtain the thermodynamic parameters listed in Table 3. Curves are the simulated DNA length dependence of the initial heat of binding with the best fit parameters at each salt concentration (simulations with different CEE assumptions are indistinguishable from each other). (C) Data from (B) were re-plotted as a function of salt concentration. (D) Representative titrations of 34 bp DNA with HU at 0.06 M (square), 0.1 M (circle), 0.125 M (triangle), and 0.15 M (diamond) Na^+. Titration data were analyzed using the modified sequence generating function method *(10)* (Eq. 5 – 7) to obtain thermodynamic parameters listed in Table 4. Curves are simulated binding isotherms with the best fit parameters at each salt concentration for the no CEE case (black) and the model CEE case (blue).

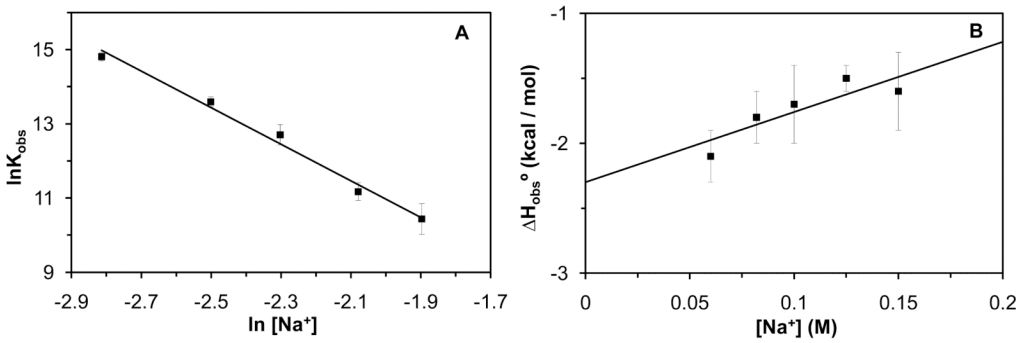

Figure 2.

Salt concentration dependences of the binding constant (A) and the binding enthalpy (B) of the 6 bp mode on 8 bp DNA in the salt concentration range 0.06 M – 0.15 M Na^+ at 15 °C. These quantities (Table 1) were determined from forward ITC titrations of 8 bp DNA with HU (Koh *et al.*, 2008: see supplemental figure 1) by fitting the titration data to a 1:1 binding model (Eq. 2 and 3). Lines represent linear regression of $\ln k_6$ with respect to $\ln[Na^+]$ (A) and of $\Delta h_6°$ with respect to $[Na^+]$ (B).

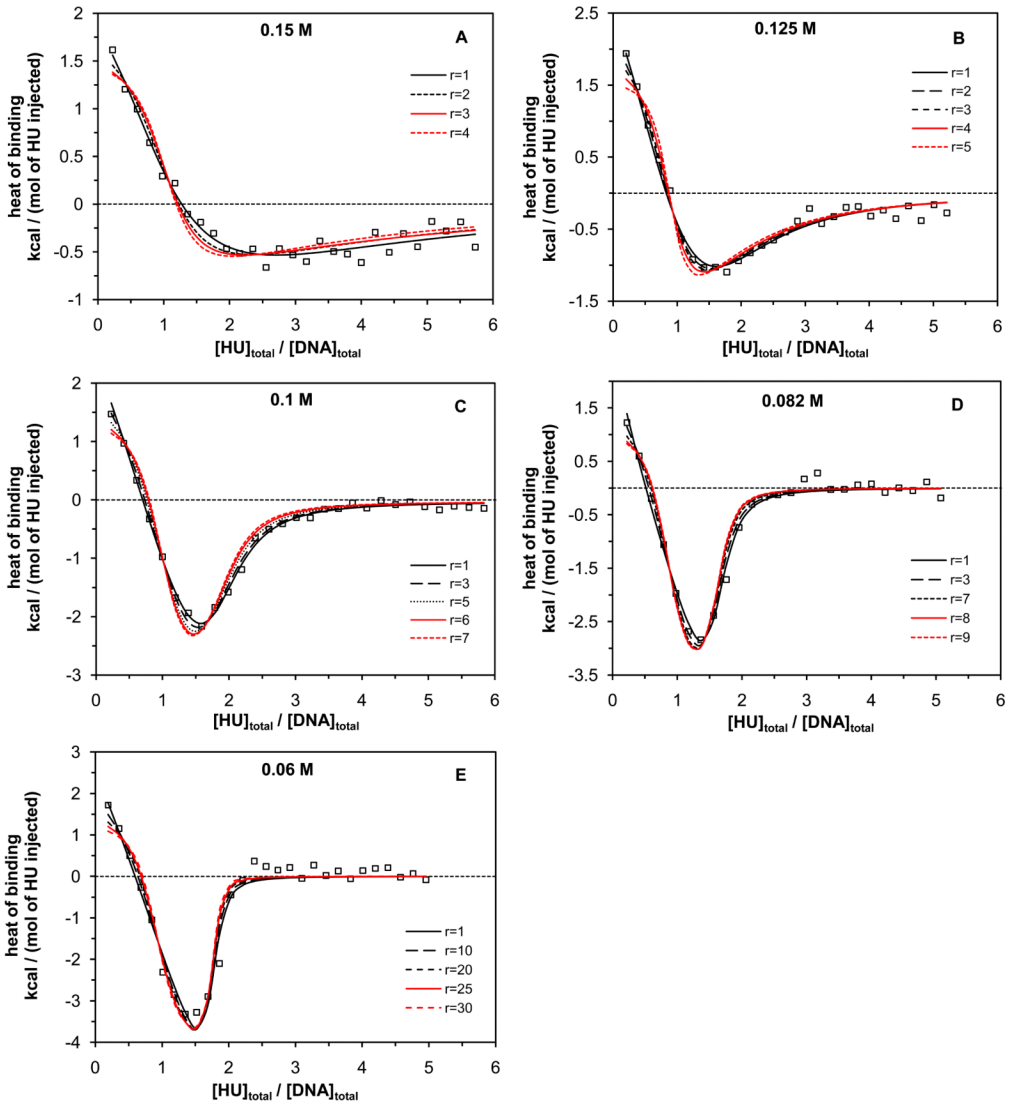

Figure 3.

Analysis of 15 bp DNA binding isotherms of HU for cases in which the binding constant of the 6 bp mode on 15 bp DNA is equal to or greater than that on 8 bp DNA at each salt concentration (i.e., $k_{6,\ 15bp}/k_{6,\ 8bp} \geq 1$; $k_{6,\ 15bp}/k_{6,\ 8bp}$ is shown as r in the figures for simplicity). A range of the ratio $k_{6,\ 15bp}/k_{6,\ bp}$ (Table 2) provides statistically and visually similar fits to the binding isotherm at each salt concentration (black curves) while the values of $k_{6,\ 5bp}/k_{6,\ 8bp}$ beyond this range significantly degrade the fits (red curves). This analysis yields the ranges of the binding constants and the binding enthalpies of the 10 bp mode and the ranges of the cooperativities and cooperativity enthalpies of the 6 bp mode (Table 2).

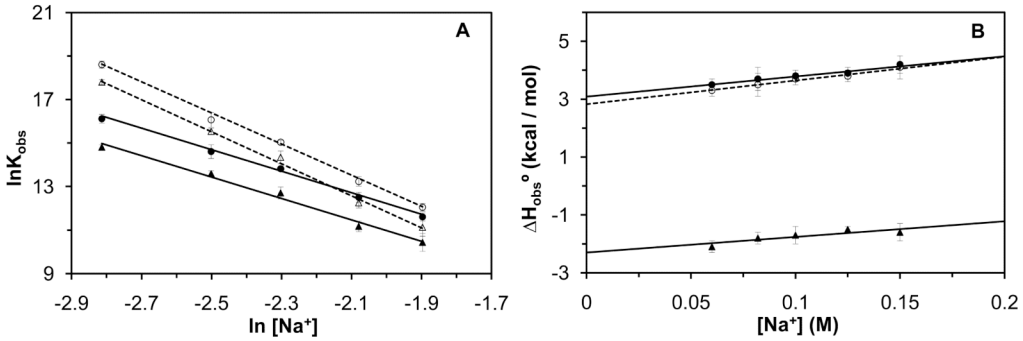

Figure 4.

Ranges of salt concentration dependences of the binding constants (A) and the binding enthalpies (B) of the 10 bp (circle) and the 6 bp (triangle) modes on 15 bp DNA in the salt concentration range 0.06 M – 0.15 M Na^+ at 15 °C. Closed and open symbols represent the cases for $k_{6,\ 15bp}/k_{6,\ 8bp}$=1 and $k_{6,\ 15bp}/k_{6,\ 8bp}$=the maximum value, respectively. Solid and dashed lines represent linear regression of $\ln k_i$ (or $\Delta h_i°$) with respect to $\ln[Na^+]$ (or $[Na^+]$) for $k_{6,\ 15bp}/k_{6,\ 8bp}$=1 and $k_{6,\ 15bp}/k_{6,\ 8bp}$=the maximum value, respectively, and define lower and upper limits of SK_{obs} on 15 bp DNA (Table 5).

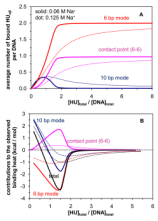

Figure 5.

(A) [HU]/[DNA] dependent population distributions (from a simulation using Eq. 4 and thermodynamic quantities for $k_{6,15bp}/k_{6,8bp}=1$ in Table 2) of the 10 bp mode (blue), the 6 bp mode (red), and the contact point between nearest neighbor HU molecules cooperatively bound in the 6 bp mode (magenta) on 15 bp DNA at 0.06 M (solid) and 0.125 M (dotted) Na^+. (B) Corresponding [HU]/[DNA] dependences of the contributions to the observed binding heat signal (black) from the 10 bp mode (blue), the 6 bp mode (red), and the contact point of the 6 bp mode (magenta) at 0.06 M (solid) and 0.125 M (dot) Na^+.

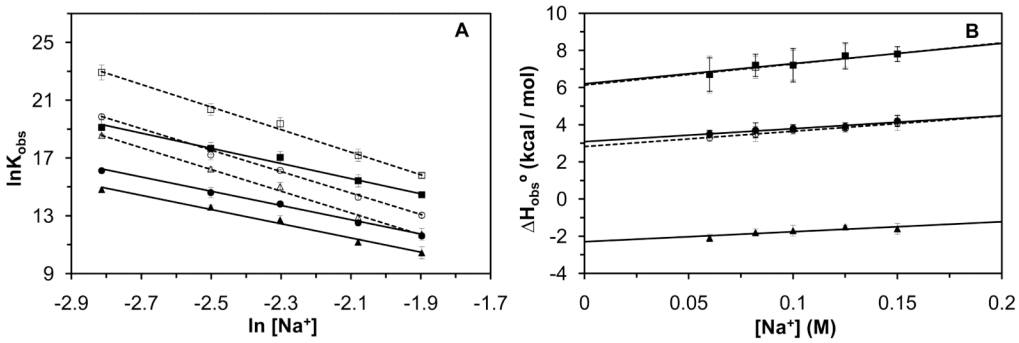

Figure 6.

Salt concentration dependences of the binding constants (A) and the binding enthalpies (B) of the 34 bp (square), the 10 bp (circle) and the 6 bp (triangle) modes on 34 bp or longer DNA in the salt concentration range 0.06 M – 0.15 M Na^+ at 15 °C. Closed and open symbols represent the no CEE and the model CEE cases, respectively. Solid and dashed lines represent linear regression of $\ln k_i$ (or $\Delta h_i°$) with respect to ln[Na^+] (or [Na+]) for these two cases, respectively (Table 5).

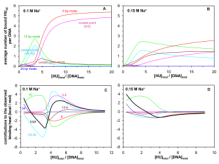

Figure 7.

(A, B) Simulated equilibrium population distributions (based on the modified SGF analysis of the 34 bp DNA binding isotherms for the model CEE case) of the 34 bp mode (blue), the 10 bp mode (green), and 6 bp mode (red), and those of the 10 bp mode contact point (cyan), the 6 bp mode contact point (magenta), and the intermode (10 bp – 6 bp) contact point (brown) on 34 bp DNA as a function of [HU]/[DNA] at 0.1 M Na^+ (A) and 0.15 M Na^+ (B). (C, D) Corresponding [HU]/[DNA] dependence of the contribution to the observed binding heat signal (black) from the heat of formation of each equilibrium species calculated in (A) and (B).

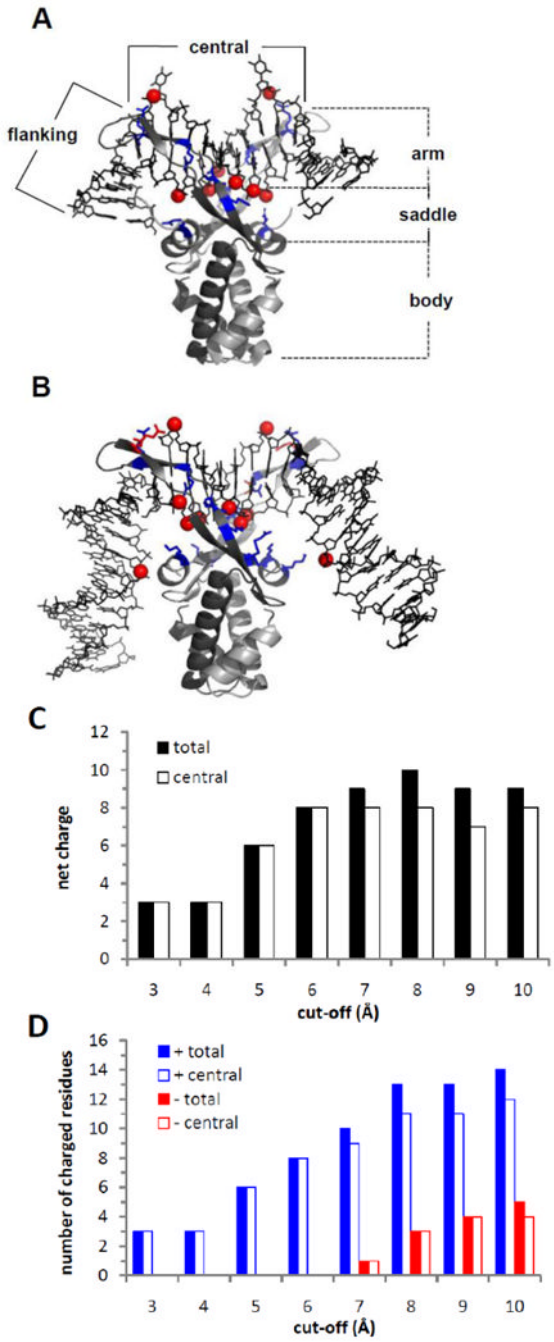

Figure 8.

(A) Distribution of charged residues in the binding interface of the complex between *Anabaena* HU and the TR3 DNA 17mer containing 3 central mismatched T:T base pairs and 4 unpaired T bases (PDB code 1P71[21]). Positively charged side chains of K, R residues (blue sticks, present in both *E.coli* and *Anabeana* HU) and negatively charged side chains of D, E residues (red sticks, present in both *E.coli* and *Anabeana* HU) which are within 8 Å of anionic DNA phosphate oxygens (red sphere) are shown. (B) A model structure of the complex between a bent 34 bp DNA containing one nick and *E.coli* HU bound in the 34 bp mode constructed from the crystal structures of the *Anabaena* HU – TR3 DNA complex (A) and of the IHF – H′ DNA complex (PDB code 1IHF[65]). Representation for distribution of

charged residues in the binding interface of the complex is the same as that in (A). (C) The net charge on the DNA binding interface of HU as a function of cut-off for the distance between the charged residues of HU and DNA phosphate oxygens. The filled and empty bars represent the net charges over the entire binding interface and the interface between the central 10 bp region of DNA and the saddle/arm region of HU, respectively. Decomposition of the net charge for each cut-off distance into the number of cationic and anionic residues is given in (D). All structural illustrations (including figure 9) were created using Pymol[88].

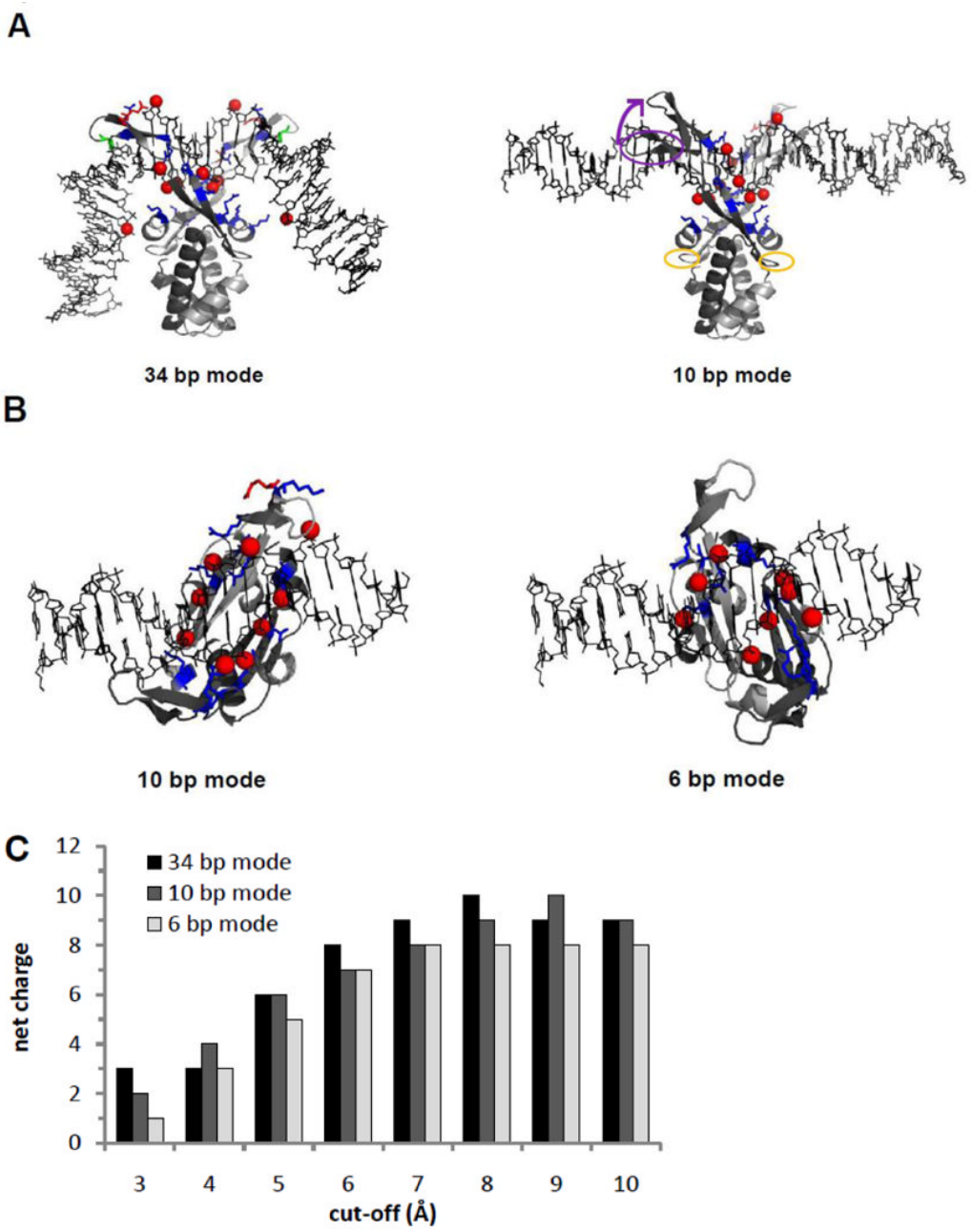

Figure 9.

(A) Model structures for the 34 bp (left panel, reproduced from fig. 8B) and the 10 bp (right panel) modes (see text for detailed discussion). Representation for distribution of charged residues in the binding interface of the complex is the same as that in figure 8. (B) Model structures for the 10 bp (left panel, a top view of the 10 bp mode shown in (A)) and the 6 bp modes (right panel). (C) The net charges on the DNA binding interfaces of HU for the three modes as a function of cut-off for the distance between the charged residues of HU and DNA phosphate oxygens.

Table 1

Thermodynamics of binding of HU to 8 bp DNA in the 6 bp mode as a function of salt concentration ([Na^+]) at 15 °C

[Na^+] (M)	k_6 (M^{-1})	$\Delta h_6°$ (kcal/mol)	$\Delta g_6°$ (kcal/mol)[c]	$T\Delta s_6°$ (kcal/mol)[d]
0.06[a]	2.7 (± 0.3) × 10^6	- 2.1 ± 0.2	- 8.5 ± 0.1	6.4 ± 0.2
0.082[a]	8.0 (± 1.1) × 10^5	- 1.8 ± 0.2	- 7.8 ± 0.1	6.0 ± 0.2
0.1[a]	3.3 (± 0.9) × 10^5	- 1.7 ± 0.3	- 7.3 ± 0.2	5.6 ± 0.3
0.125[a]	7.1 (± 1.7) × 10^4	- 1.5 ± 0.1	- 6.4 ± 0.1	4.9 ± 0.2
0.15[b]	3.4 (± 1.4) × 10^4	- 1.6 ± 0.3	- 6.0 ± 0.2	4.4 ± 0.3

[a] ITC data from Koh *et al.* (2008) were analyzed using the 1:1 binding model. Uncertainties were determined from at least three independent measurements.

[b] From Koh *et al.* (2008)

[c] $\Delta g_6° = -RT \ln k_6$.

[d] $T\Delta s_6° = \Delta h_6° - \Delta g_6°$.

Table 2

Thermodynamics of binding of HU to 15 bp DNA in the 10 bp and the 6 bp modes as a function of salt concentration ([Na^+]) at 15 °C[a]

[Na^+] (M)	$k_{6,\ 15bp}/k_{6,8bp}$[b]	k_6 (M^{-1})	$\Delta h_6°$ (kcal/mol)	k_{10} (M^{-1})	$\Delta h_{10}°$ (kcal/mol)	$\Delta g_{10}°$[d] (kcal/mol)	$T\Delta s_{10}°$[e] (kcal/mol)	ω_6	$\Delta h_{\omega 6}°$ (kcal/mol)
0.06	1	2.7×10^6	- 2.1	$1.0 (\pm 0.2) \times 10^7$	3.5 ± 0.2	- 9.2 ± 0.1	12.7 ± 0.2	54.6 ± 8.5	1.9 ± 0.3
	20	5.4×10^7	- 2.1	$1.2 (\pm 0.2) \times 10^8$	3.3 ± 0.2	- 10.6 ± 0.1	13.9 ± 0.2	4.4 ± 2.0	2.5 ± 0.5
0.082	1	8.0×10^5	- 1.8	$2.2 (\pm 0.7) \times 10^6$	3.7 ± 0.4	- 8.4 ± 0.2	12.1 ± 0.4	49.5 ± 8.7	1.2 ± 0.4
	7	5.6×10^6	- 1.8	$9.5 (\pm 3.3) \times 10^6$	3.5 ± 0.4	- 9.2 ± 0.2	12.7 ± 0.4	5.4 ± 1.2	1.6 ± 0.5
0.1	1	3.3×10^5	- 1.7	$1.0 (\pm 0.1) \times 10^6$	3.8 ± 0.2	- 7.9 ± 0.1	11.7 ± 0.2	44.0 ± 6.7	1.5 ± 0.4
	5	1.7×10^6	- 1.7	$3.4 (\pm 0.3) \times 10^6$	3.7 ± 0.2	- 8.6 ± 0.1	12.3 ± 0.2	6.9 ± 1.0	1.9 ± 0.4
0.125	1	7.1×10^4	- 1.5	$2.7 (\pm 0.6) \times 10^5$	3.9 ± 0.2	- 7.2 ± 0.1	11.1 ± 0.2	36.2 ± 9.8	1.2 ± 0.3
	3	2.1×10^5	- 1.5	$5.6 (\pm 1.2) \times 10^5$	3.8 ± 0.2	- 7.6 ± 0.1	11.4 ± 0.2	6.1 ± 1.9	1.3 ± 0.2
0.15[c]	1	3.4×10^4	- 1.6	$1.1 (\pm 0.2) \times 10^5$	4.2 ± 0.3	- 6.6 ± 0.1	10.8 ± 0.3	24.0 ± 11.0	- 0.3 ± 1.0
	2	6.8×10^4	- 1.6	$1.7 (\pm 0.3) \times 10^5$	4.1 ± 0.4	- 6.9 ± 0.1	11.0 ± 0.4	7.2 ± 3.8	- 0.8 ± 1.4

[a] Analysis floats k_{10}, $\Delta h_{10}°$, ω_6, and $\Delta h_{\omega 6}°$, fixing k_6 and $\Delta h_6°$ as indicated. Uncertainties were determined from at least three independent measurements.

[b] Minimum and maximum values of ratio of the binding constant of the 6 bp mode on 15 bp DNA to that on 8 bp DNA (Table 1) at each salt concentration yielding statistically and visually similar fits to 15 bp DNA binding isotherms

[c] Reanalysis of data of Koh *et al.* (2008)

[d] $\Delta g_{10}° = -RT \ln k_{10}$.

[e] $T\Delta s_{10}° = \Delta h_{10}° - \Delta g_{10}°$.

Table 3

Thermodynamics of binding of HU to 34 bp and longer DNA in the 34 bp mode (and the other two modes) as a function of salt concentration ([Na^+]) at 15 °C obtained from analysis of initial heat of binding (34 bp, 38 bp, and 160 bp DNA)[a]

[Na^+] (M)		$k_{6,15bp}/k_{6,8bp}$	$k_{6,34bp}/k_{6,15bp}$	$k_{10,34bp}/k_{10,15bp}$	k_{34}/k_6	k_{34}/k_{10}	k_{34} (M^{-1})	$\Delta h_{34}°$ (kcal/mol)	$\Delta g_{34}°$[e] (kcal/mol)	$T\Delta s_{34}°$ [f] (kcal/mol)
0.06	no CEE[b]	1	1	1	74.1 ± 28.7	20.0 ± 7.7	2.0 (± 1.0) × 10^8	6.7 ± 0.9	- 10.9 ± 0.3	17.6 ± 0.9
	model CEE[c]	20	2.1	3.4	78.6 ± 30.3	21.4 ± 8.1	9.0 (± 4.5) × 10^9	6.7 ± 1.0	- 13.1 ± 0.3	19.8 ± 1.0
0.082	no CEE[b]	1	1	1	58.8 ± 22.8	21.4 ± 8.2	4.7 (± 1.8) × 10^7	7.2 ± 0.6	- 10.1 ± 0.2	17.3 ± 0.6
	model CEE[c]	7	2.0	3.1	62.2 ± 24.1	23.4 ± 9.0	7.0 (± 2.8) × 10^8	7.1 ± 0.6	- 11.7 ± 0.2	18.8 ± 0.6
0.1	no CEE[b]	1	1	1	75.8 ± 26.4	25.0 ± 8.3	2.5 (± 1.1) × 10^7	7.2 ± 0.9	- 9.8 ± 0.3	16.9 ± 0.9
	model CEE[c]	5	2.0	3.0	78.4 ± 27.2	25.4 ± 8.4	2.6 (± 1.1) × 10^8	7.2 ± 0.8	- 11.1 ± 0.2	18.3 ± 0.8
0.125	no CEE[b]	1	1	1	70.4 ± 24.4	18.5 ± 6.2	5.0 (± 2.2) × 10^6	7.7 ± 0.7	- 8.8 ± 0.3	16.5 ± 0.7
	model CEE[c]	3	1.9	2.9	73.8 ± 25.6	18.0 ± 6.0	2.9 (± 1.3) × 10^7	7.7 ± 0.6	- 9.8 ± 0.2	17.5 ± 0.6
0.15[d]	no CEE[b]	1	1	1	55.9 ± 10.3	17.3 ± 2.9	1.9 (± 0.4) × 10^6	7.8 ± 0.4	- 8.3 ± 0.1	16.1 ± 0.4
	model CEE[c]	2	1.8	2.7	58.3 ± 10.8	15.7 ± 2.6	7.2 (± 1.2) × 10^6	7.8 ± 0.4	- 9.0 ± 0.1	16.8 ± 0.4

[a] Analysis floats k_{34}/k_6 and Δh_{34}, fixing Δh_{10} and Δh_6 (Table 2), and k_{10}/k_6 as dictated by the CEE assumptions.

[b] k_6 and k_{10} assumed to be independent of DNA length

[c] Increases in k_6 and k_{10} from 8 bp to 15 bp DNA and from 15 bp to 34 bp DNA estimated from oligo-model of the CEE[56]

[d] Reanalysis of data of Koh *et al.* (2008)

[e] $\Delta g_{34}° = -RT \ln k_{34}$.

[f] $T\Delta s_{34}° = \Delta h_{34}° - \Delta g_{34}°$.

Table 4

Cooperativities and cooperativity enthalpies involving the HU 10 bp mode as a function of [Na^+] obtained from analysis of the entire 34 bp DNA binding isotherms using the modified sequence generating function method [a]

CEE assumption	[Na^+] (M)	ω_{10}	$\omega_{10/6}$	$\Delta h_{\omega 10}$ ° (kcal/mol)	$\Delta h_{\omega 10/6}$° (kcal/mol)
no CEE	0.06	54.2 ± 17.8	41.7 ± 18.9	- 6.8 ± 0.5	- 2.9 ± 1.5
	0.1	44.3 ± 9.9	12.7 ± 5.4	- 5.4 ± 0.4	- 2.8 ± 1.2
	0.125	28.6 ± 8.5	4.2 ± 2.9	- 4.9 ± 0.3	- 4.1 ± 2.0
	0.15	17.5 ± 9.9	10.8 ± 7.1	- 3.0 ± 1.1	- 3.0 ± 1.7
model CEE	0.06	16.9 ± 7.7	11.1 ± 5.7	- 6.9 ± 0.8	- 2.4 ± 1.3
	0.1	20.1 ± 3.4	5.0 ± 2.9	- 5.3 ± 0.4	- 3.1 ± 1.3
	0.125	12.2 ± 3.8	2.5 ± 1.5	- 5.2 ± 0.4	- 3.6 ± 2.0
	0.15	13.6 ± 9.1	5.6 ± 3.7	- 3.4 ± 1.1	- 2.8 ± 1.2

[a] Values of k_{34}, k_{10}, k_6, Δh_{34}°, Δh_{10}°, Δh_6°, ω_6, and $\Delta h_{\omega 6}$° determined from analyses of 8 bp and 15 bp DNA binding isotherms and of initial heats of binding to 34 bp, 38 bp and 160 bp DNA for different assumptions of CEEs (Tables 1 – 3) were used in this analysis.

Table 5

Ranges of salt concentration dependences of the binding constants $(Sk_i \equiv \frac{d\ln k_i}{d\ln[Na^+]})$ and binding enthalpies $(\frac{d\Delta h_i^\circ}{d[Na^+]})$ of the three nonspecific DNA binding modes of HU at 15 °C

Mode	Sk_i 8 bp DNA	Sk_i 15 bp DNA		Sk_i 34 bp and longer DNA	
		$k_{6,15bp}/k_{6,8bp} = 1$	$k_{6,15bp}/k_{6,8bp}$ = max.	no CEE	model CEE
34 bp mode	-	-	-	- 5.3 ± 0.5	- 7.8 ± 0.7
10 bp mode	-	- 4.9 ± 0.3	- 7.2 ± 0.4	- 4.9 ± 0.3	- 7.4 ± 0.4
6 bp mode	- 4.9 ± 0.3	- 4.9 ± 0.3	- 7.4 ± 0.4	- 4.9 ± 0.3	- 7.5 ± 0.4

Mode	$\frac{d\Delta h_i^\circ}{d[Na^+]}$ 8 bp DNA	$\frac{d\Delta h_i^\circ}{d[Na^+]}$ 15 bp DNA		$\frac{d\Delta h_i^\circ}{d[Na^+]}$ 34 bp and longer DNA	
		$k_{6,15bp}/k_{6,8bp} = 1$	$k_{6,15bp}/k_{6,8bp}$ = max.	no CEE	model CEE
34 bp mode	-	-	-	10.9 ± 4.6	11.4 ± 4.9
10 bp mode	-	7.0 ± 2.0	8.2 ± 2.1	7.0 ± 2.0	8.2 ± 2.1
6 bp mode	5.4 ± 2.2	5.4 ± 2.2	5.4 ± 2.2	5.4 ±2.2	5.4 ±2.2